Immune pathway upregulation and lower genomic instability distinguish EBV-positive nodal T/NK-cell lymphoma from ENKTL and PTCL-NOS

Cho Mar Myint Wai,[1*] Shangying Chen,[2*] The Phyu,[1] Shuangyi Fan,[1] Sai Mun Leong,[1] Wenning Zheng,[3] Louis Ching Yi Low,[1] Shoa-Nian Choo,[1] Chi-Kuen Lee,[1] Tae-Hoon Chung,[3] Kenneth Hon Kim Ban,[2] Soumita Ghosh,[3] Stefanus Lie,[3] Seiichi Kato,[4,5] Shigeo Nakamura,[4] Emiko Takahashi,[6] Young-Hyeh Ko,[7] Joseph D. Khoury,[8] Shih-Sung Chuang,[9] Rex K.H. Au-Yeung,[10] Soo-Yong Tan,[1,11] Soon-Thye Lim,[12] Choon-Kiat Ong,[13-15] Yong-Howe Ho,[16] Li Mei Poon,[17] Sanjay de Mel,[17] Anand D. Jeyasekharan,[3] Wee-Joo Chng,[3,17,18] Franziska Otto,[19] Leticia Quintanilla-Martinez,[19] Federica Zanardi,[20] Fabio Iannelli,[20] Claudio Tripodo,[21] Jason J. Pitt[3] and Siok-Bian Ng[1,3,11]

[1]Department of Pathology, Yong Loo Lin School of Medicine, National University of Singapore, Singapore; [2]Department of Biochemistry, Yong Loo Lin School of Medicine, National University of Singapore, Singapore; [3]Cancer Science Institute of Singapore, National University of Singapore, Singapore; [4]Department of Pathology and Laboratory Medicine, Nagoya University Hospital, Nagoya, Japan; [5]Department of Pathology and Molecular Diagnostics, Aichi Cancer Center Hospital, Nagoya, Japan; [6]Department of Pathology, Aichi Medical University Hospital, Nagakute, Japan; [7]Department of Pathology, Samsung Medical Center, Sungkyunkwan University, Seoul, Korea; [8]Department of Hematopathology, The University of Texas MD Anderson Cancer Center, Houston, TX, USA; [9]Department of Pathology, Chi-Mei Medical Center, Tainan, Taiwan; [10]Department of Pathology, Queen Mary Hospital, The University of Hong Kong, Hong Kong SAR, China; [11]Department of Pathology, National University Hospital, National University Health System, Singapore; [12]Lymphoma Genomic Translational Research Laboratory, National Cancer Center Singapore, Singapore; Division of Medical Oncology, National Cancer Center Singapore, Singapore; [13]Lymphoma Genomic Translational Research Laboratory, Division of Medical Oncology, National Cancer Centre Singapore, Singapore; [14]Duke-NUS Medical School, Singapore; [15]Genome Institute of Singapore, A*STAR (Agency for Science, Technology and Research), Singapore; [16]Department of Pathology, Tan Tock Seng Hospital, Singapore; [17]Department of Hematology-Oncology, National University Cancer Institute Singapore, National University Hospital, National University Health System, Singapore;[18]Department of Medicine, Yong Loo Lin School of Medicine, National University of Singapore, Singapore; [19]Institute of Pathology and Neuropathology, Eberhard Karls University of Tübingen and Comprehensive Cancer Center, Tübingen University Hospital, Tübingen, Germany; [20]Bioinformatics Unit, IFOM - the FIRC Institute of Molecular Oncology, Milan, Italy and [21]Tumor Immunology Unit, University of Palermo School of Medicine, Palermo, Italy

CMMW and SC contributed equally as co-first authors.

Correspondence:

Siok-Bian Ng (lead contact)
patnsb@nus.edu.sg

Jason J. Pitt
jason.j.pitt@nus.edu.sg

Immune pathway upregulation and lower genomic instability distinguish EBV-positive nodal T/NK-cell lymphoma from ENKTL and PTCL-NOS

Cho Mar Myint Wai,[1,*] Shangying Chen,[2,*] The Phyu,[1] Shuangyi Fan,[1] Sai Mun Leong,[1] Wenning Zheng,[3] Louis Ching Yi Low,[1] Shoa-Nian Choo,[1] Chi-Kuen Lee,[1] Tae-Hoon Chung,[3] Kenneth Hon Kim Ban,[2] Soumita Ghosh[3], Stefanus Lie,[3] Seiichi Kato,[4,5] Shigeo Nakamura,[4] Emiko Takahashi,[6] Young-Hyeh Ko,[7] Joseph D. Khoury,[8] Shih-Sung Chuang,[9] Rex K.H. Au-Yeung,[10] Soo-Yong Tan,[1,11] Soon-Thye Lim,[12] Choon-Kiat Ong,[13-15] Yong-Howe Ho,[16] Li Mei Poon,[17] Sanjay de Mel,[17] Anand D. Jeyasekharan,[3] Wee-Joo Chng,[3,17,18] Franziska Otto,[19] Leticia Quintanilla-Martinez,[19] Federica Zanardi,[20] Fabio Iannelli,[20] Claudio Tripodo,[21] Jason J. Pitt,[3,†] and Siok-Bian Ng[1,3,11,†,Δ]

Author Affiliations:
[1]Department of Pathology, Yong Loo Lin School of Medicine, National University of Singapore, Singapore;
[2] Department of Biochemistry, Yong Loo Lin School of Medicine, National University of Singapore, Singapore;
[3]Cancer Science Institute of Singapore, National University of Singapore, Singapore;
[4]Department of Pathology and Laboratory Medicine, Nagoya University Hospital, Nagoya, Japan;
[5]Department of Pathology and Molecular Diagnostics, Aichi Cancer Center Hospital, Nagoya, Japan;
[6]Department of Pathology, Aichi Medical University Hospital, Nagakute, Japan;
[7]Department of Pathology, Samsung Medical Center, Sungkyunkwan University, Seoul, Korea;
[8]Department of Hematopathology, The University of Texas MD Anderson Cancer Center, Houston, TX;
[9]Department of Pathology, Chi-Mei Medical Center, Tainan, Taiwan;
[10]Department of Pathology, Queen Mary Hospital, The University of Hong Kong, Hong Kong SAR, China;
[11]Department of Pathology, National University Hospital, National University Health System, Singapore;
[12]Lymphoma Genomic Translational Research Laboratory, National Cancer Centre Singapore, Singapore; Division of Medical Oncology, National Cancer Centre Singapore, Singapore;
[13]Lymphoma Genomic Translational Research Laboratory, Division of Medical Oncology, National Cancer Centre Singapore, Singapore;
[14]Duke-NUS Medical School, Singapore, Singapore;
[15]Genome Institute of Singapore, A*STAR (Agency for Science, Technology and Research), Singapore, Singapore;
[16]Department of Pathology, Tan Tock Seng Hospital, Singapore;
[17]Department of Hematology-Oncology, National University Cancer Institute Singapore, National University Hospital, National University Health System, Singapore;
[18]Department of Medicine, Yong Loo Lin School of Medicine, National University of Singapore, Singapore;
[19]Institute of Pathology and Neuropathology, Eberhard Karls University of Tübingen and Comprehensive Cancer Center, Tübingen University Hospital, Tübingen, Germany;
[20]Bioinformatics Unit, IFOM - the FIRC Institute of Molecular Oncology, Milan, Italy
[21]Tumor Immunology Unit, University of Palermo School of Medicine, Palermo, Italy

*These authors contributed equally to this work
†Corresponding authors
ΔLead contact

Corresponding authors:

Ng Siok-Bian, Associate Professor and Senior Consultant, National University of Singapore
DID: (65) 67724709 | patnsb@nus.edu.sg

Jason J Pitt, Special Fellow, Cancer Science Institute of Singapore, NUS
DID: (65) 65168055 | jason.j.pitt@nus.edu.sg

Competing Interests

Supplementary Methods

Study Cohort

The study group included 150 adult patients with no known immune deficiency and diagnosed between 1994 to 2018. The diagnosis of ENKTL (n=89), PTCL-EBV (n=25) and PTCL-NOS (n=36) were reviewed by 2 hematopathologists based on the 2017 WHO lymphoma classification.[1] ENKTL cases were positive for CD3 and/or CD2, at least one cytotoxic marker (TIA1 or granzyme B) and EBV-encoded small RNAs (EBER). Systemic and cutaneous EBV-positive T/NK lymphoproliferative diseases occurring in children, (such as systemic EBV-positive T-cell lymphoma of childhood, aggressive NK-cell leukemia, and chronic active EBV infection of T/NK type), angioimmunoblastic T-cell lymphomas and EBV-positive B cell lymphomas were excluded. As expected, ENKTL cases in our study involve mostly extranodal sites (n=86) and only a minority involve nodal (n=3) sites. The diagnostic inclusion criteria for EBV+ PTCL were i) positivity for at least one T cell marker (CD3, CD4, CD8, CD2, CD5, CD7, CD43, UCHL1, TCRB and/or TCRG), ii) the absence of B-cell markers (CD20, CD79A) and iii) positive EBV expression. The diagnostic criteria for PTCL-EBV and the distinction from ENKTL based on tumor site, nasal involvement, expression of CD8 and CD56 markers, and T vs NK cell lineage are listed in Table S1. The diagnosis of PTCL-NOS was made after other specific subtypes of PTCL have been excluded, including anaplastic large cell lymphoma and PTCL with T-follicular helper phenotype, including angioimmunoblastic T cell lymphoma. PTCL-NOS was further categorized into cytotoxic (n=19) and non-cytotoxic cases (n=15). Cytotoxicity was defined as the positive expression of at least one cytotoxic markers, TIA1 and granzyme B.

Some cases and data have been previously reported,[2] including ENKTL (n=47), PTCL-EBV (n=19) and Oncoscan data (n=41). Clinical data including age, sex, disease type, stage, International Prognostic Index (IPI) score, expression of CD4, CD8 and CD56, T or NK lineage, treatment and overall survival of all cases were summarized in Table S2A and detailed immunophenotype of PTCL-EBV summarized in Table S2B.

As previously described[2], T-cell lineage is established based on a combination of positive expression of TCRB/TCRG proteins, T-cell markers, T-cell monoclonality, absence of B-cell monoclonality and/or lack of B-cell marker expression. Seventeen of 25 PTCL-EBV showed

positive expression for TCR proteins and/or T-cell monoclonality. The remaining 8 cases were either negative for TCR proteins and/or had incomplete T-cell clonality data but were positive for ≥ one T-cell marker and negative for ≥ one B-cell marker, compatible with PTCL. NK-cell lineage was assigned based on a combination of a) CD56+/CD8- phenotype, b) lack of TCRB and TCRG expression by IHC and/or c) germline TCRG by PCR. Refer to flow chart illustrating T vs NK cell lineage determination (Fig S15).

DNA/RNA extraction

Total RNA and DNA from FFPE tissue samples were extracted by using the RecoverAll™ Total Nucleic Acid Isolation Kit for FFPE Invitrogen™ and from cell lines and primary T and NK cells were extracted by using Qiagen's miRNeasy® Mini Kit and Qiagen DNeasy Blood & Tissue Kit (Qiagen, Hilden, Germany) following manufacturer's protocol.

Gene expression profiling (GEP)

The quality of total RNA isolated from FFPE tissue samples of 35 ENKTL cases, 23 PTCL-EBV cases, 26 PTCL-NOS cases were determined using spectrophotometric methods (NanoDrop, Thermo Fisher Scientific, Waltham, MA, U.S.A). Briefly, 30 ng of total RNA was reverse transcribed to cDNA. This double-stranded cDNA was then amplified via in vitro transcription (IVT) to produce cRNA which was then purified and subjected to 2nd-cycle single-stranded sense cDNA synthesis and later fragmented, labeled, and hybridized to GeneChip® Clariom D Assay (Human) Array. Arrays were then scanned using an Affymetrix 3000 7G scanner. The scanned images were inspected for hybridization efficiency and CEL files generated from AGCC (GeneChip Command Console Software).

Gene expression data were normalized with the robust multi-array average (RMA) algorithm through the "oligo" package (1.48.0) in R (ver 3.6). The gene expression values were further standardized by the Z-score transformation method.[3] Differentially expressed genes (DEG) were identified via Bayesian adjusted t-statistics from the linear models implemented in the "limma"

package (v3.40.6). Genes with normal $P<0.01$ and adjusted $P<0.05$ were considered DEGs. Any DEGs (probes) not present in the Consensus CDS (CCDS) database (v15) were discarded. Heatmaps were generated with "ComplexHeatmap" (v2.0.0). Unsupervised hierarchical clustering was performed using Spearman distance and Ward.D2's linkage.

Copy number analysis

DNA was extracted from FFPE samples of 34 ENKTL cases, 14 PTCL-EBV cases and 29 PTCL-NOS cases with 80ng of input DNA used for each sample. Briefly, the genomic DNA targets were annealed to molecular inversion probes (MIP) followed by gap-filling with dNTPs (ATs or GCs) to circularize the MIP probes. Non-circularized probes were removed by exonuclease I treatment. Circularized probes were then cleaved and released from the DNA targets and inverted to the correct orientation for the first round of PCR amplification before assessing for successful amplification on 4% E-Gel® 48 (Invitrogen). Thereafter, 2uL of PCR product was used for the second round of PCR amplification followed by restriction digestion with HaeIII.Complete digestion was confirmed on the 4% E-Gel® 48 before digested products were hybridized to the Affymetrix OncoScanCNV array containing 328,000 tags for 16 to 18 hours at 49°C, 60 rpm. Finally, the arrays were washed and stained in GeneChip® Fluidics Station 450 prior to scanning using the GeneChip® 3000 7G scanner. The CEL files were imported into OncoScan® Console 1.3 software (ThermoFisher Scientific, Waltham, MA, USA) for analysis.

Calculation of GI- and HRD scores

Taking the segmentation output from OncoScan® Console, GI score was defined by the ratio of the total length of regions with a copy number other than 2 to a constant of 3.3×10^9, according to the previous studies.[4,5] Somatic homologous recombination deficiency (HRD) scores were calculated based on published methods[5] using the output of allele-specific segmentation which is generated via "EaCoN" (ver 0.3.5).[6] Briefly, HRD was defined based on four independent signatures. The first three HRDs were based on loss of heterozygosity (LOH) corresponding to the number of LOH segments (LOH HRD), telomere allelic imbalance (AIL) which is the sum of

regions of allelic imbalance (AIL HRD) and large-scale state transitions (LST) which is the number of breakpoints between regions longer than 10Mb (LST HRD). The fourth method is defined as (LOH HRD + AIL HRD + LST HRD)/3.

Analysis of segmentation numbers and size distribution

The total number of copy number segments identified by OncoScan® Console were calculated for each case. Only segments containing more than 10 probes are considered and segments with a median log2 ratio above 0.1 are considered "gain" or below -0.1 are considered "loss". The Kruskal-Wallis test was used to compare complexity between three groups while Mann-Whitney U tests were used for pairwise comparisons.

The size of the segment was calculated and analysed using the graphical method geom_density function of the ggplot2 package in R software, with the segment size on x-axis with log-transformed scaling and the density of samples on the y-axis. Pairwise comparisons of CNA size distributions among three groups was performed using a two-sample Kolmogorov-Smirnov (KS) test.

GISTIC analysis

Recurrent copy number alterations were evaluated by the Genomic Identification of Significant Targets in Cancer (GISTIC).[7] GISTIC analysis was performed using the Java GISTIC implementation version 2.0.22 in the Ubuntu 18.04.2 LTS system. GISTIC identified regions of genome that are significantly amplified or deleted across a set of cancer samples. Each amplified or deletion event is assigned a G-score that considers the frequency of occurrence among the sample set. False Discovery Rate q-values are then calculated for each region of gain or loss. Segmentation results of the lymphoma samples from OncoScan® Console were used for GISITC analysis. Our GISTIC2.0 was run with parameters -ta 0.1 -td -0.1 -conf 0.75 -broad 1. The standard q value of 0.25 was used to define significant regions of recurrent copy-number variation. Genomic coordinates used in this study are from human GENCODE Hg19 genome build.

Based on the all-lesion file from GISTIC running with all lymphoma samples, we further compared the differences of the sample CNA status in the significant gain/loss regions among the three disease groups using the Kruskal-Wallis test. The number and frequency of samples in the significant gain/loss regions were calculated for the three disease groups, ENKTL, PTCL-EBV and PTCL-NOS respectively.

Network and enrichment analyses

DEGs were submitted to the STRING web portal to identify known gene-gene interactions (including protein-protein interactions [PPI]) using STRING's default scoring metrics. For each submitted gene set, enrichment for PPI as well as Biological Process and Cellular Component gene ontology terms were calculated. For hub genes within the resulting STRING gene-gene interaction networks, we calculated the betweenness centrality score for each DEG in Cytoscape (v 3.8.0). The ten genes with the highest scores were retained for each set of DEGs.

For Gene Set Enrichment Analyses (GSEA)[8] (v 4.0.3), submitted gene lists were either ranked by Spearman's Rho or t-statistic — the latter a surrogate for differential gene expression between two groups (e.g. PTCL-EBV vs ENKTL). All gene sets (e.g. Hallmark Gene Sets and five sets of NFkB transcriptional target genes) were obtained from MSigDB.[9] GSEA was run using default parameter settings. Gene sets with an fdr q-value < 0.05 were considered significant.

Tumor content and tumor microenvironment (TME)

The tumor content for the 3 groups of tumor was computed using "EaCoN" (ver 0.3.5) from Oncoscan data. For TME, the proportion of immune cell types was determined by deconvolution of normalized transcriptome with CIBERSORTx[10] setting the B-mode as batch correction mode and 500 permutations. For the analysis, a signature matrix of 13 cell types was used and this was generated after removal of T and NK cell types from the CIBERSORT LM22 matrix.

To compare the similarity of the composition of immune cells in the three disease groups, cosine similarity value is calculated for each group pair (ENKTL vs PTCL-EBV, ENKTL vs PTCL-NOS and PECL-EBV vs PTCL-NOS) using "lsa" (v0.73.2) R package based on the data of the mean fraction (%) of the immune cells in the disease groups. The cosine similarity of data sets will range from 0 to 1, with higher similarity value indicating greater similarity level.

Correlation analysis of expression level between PD-L1 and IFNγ, NFkB signaling and IL6_JAK_STAT signaling

The associated genes in the IL6_JAK_STAT signaling and NFkB signaling were collected from Molecular Signatures Database (MSigDB) Hallmarks gene sets (v7.2). We found five gene sets depicting targets of NFkB signaling, and the union was used when calculating the NFkB expression index. The expression index of the NFkB and IL6_JAK_STAT signaling were summarized by median expression of all genes within the set.[11] Correlation of expression levels between PD-L1 and IFNγ, NFkB signaling and IL6_JAK_STAT signaling was performed in R using Spearman's method with Rho and *P* values calculated.

EBV miRNA qPCR analysis

Quantitative reverse transcription PCR (RT-qPCR) analysis of EBV-miRNA expression was performed using IDEAL miRNA qPCR assays (MiRXES, Singapore) according to manufacturer's instructions. Briefly, multiplex reverse transcription was carried out in 10µL reaction volume containing 100 nM miRNA specific stem-loop RT primers, 1× RT buffer, 1x reverse transcriptase and 50ng total template RNA. The reaction was conducted at 42°C for 30min, followed by heat-inactivation at 95°C for 5 min using a thermal cycler (Eppendorf). Synthesized cDNA was diluted 10 times in nuclease free water before it was subjected to RT qPCR in a total volume of 10uL in 1x IDEAL miRNA qPCR Master Mix with 1x miRNA specific qPCR assay (MiRXES, Singapore). RT qPCR was performed on QuantStudio™ 5 System (ThermoFisher Scientific, Waltham, MA, USA) in a 384-well plate. Thermocycling of cDNAs was performed with 10 min of initial denaturation at 95°C and 4 min of polymerase activation at 40°C, followed by 40 cycles of 10 s denaturation at 95°C and 30 s annealing / extension at 60°C. Each cDNA sample was run in

triplicate for the qPCR. Relative gene expressions (ΔCt) were obtained by normalizing each gene Ct to the mean Ct of housekeeping genes. Among the four housekeeping genes (miR-423-5p, miR-320c, U6 and 5S) included in the qPCR assay, U6 and S5 were selected as housekeeping control (reference) as they were highly expressed with least variability across all the analysed samples (Data not shown). The differences of expression (ΔCt) for each EBV-miRNA between the ENKTL and PTCL-EBV were evaluated by two sample t-test and p-value was calculated and *P*<0.05 was considered significant (Table S13). Cluster analysis and heatmap visualization of all EBV-miRNA were conducted with the ComplexHeatmap package (v 2.0.0) in R. The unsupervised hierarchical clustering of the patients was performed with Euclidean distance and complete linkage for clustering.

Correlation and functional analysis of predicted targets associated with differentially expressed EBV-miRNAs

Both known and predicted target genes of the differently expressed EBV-miRNAs were obtained from VIRmiRNA.[12] Twenty-two out 32 differentially expressed (DE) EBV-miRNA and 1677 EBV miRNA-target pairs were found in the database, of which 1580 were unique gene targets. Expression correlation between EBV-miRNA (ΔCt) and its target gene(s) (mRNA expression) was evaluated by Spearman's method. Negatively correlated pairs with an adjusted $p < 0.05$ were considered bona fide EBV-miRNA-target pairs. This resulted in 172 EBV miRNA-target pairs and 163 unique targets (Table S14). These unique targets were then used in the subsequent analyses.

The expression index (median expression value) of the aforementioned 163 target genes was calculated for each ENKTL and PTCL-EBV sample.[11] The comparison of the expression index between ENKTL and PTCL-EBV was performed by Mann-Whitney U test with ggpubr package (v 0.2.1) in R.

EBV latency analysis

RT-qPCR analysis of EBV genes were performed on PTCL-EBV (n=13) and ENTKL (n=6) FFPE samples. 1µg of RNA was reverse transcribed to cDNA using a high-capacity cDNA reverse

transcription kit (Applied Biosystems, Thermo Fisher Scientific). Primers for RT-qPCR are LMP1 F: 5'-GTCCTGTGGGCCATTGTC-3', R: 5'- CCCACTCTGCTCTCAAAACC-3', LMP2 F: 5'-GACATGAAGAGCACGAAGAGC-3', R: 5'- TTCTCATGCTCCTATGGACACTT-3', EBNA1 F:5'-GAGAAGGCCCAAGCACTG-3', R: 5'- CTCCTTGACCACGATGCTTT-3'. Cycling conditions were as follows: after an initial denaturation step at 95°C for 20 sec, amplification was performed by using 40 cycles of denaturation (95°C, 1 s), annealing (60°C, 20 s), and melt-curve stage (95°C, 1 s; 60°C, 20 s; 95°C, 1 s). EBV latency is categorized as follows: i) Latency 1 - expression of EBNA1 alone, ii) Latency 2 - expression of EBNA1, LMP1, LPM2A, iii) Latency 3 - expression of EBNA1, LMP1, LMP2A and EBNA2 (Table S12).

Fluorescence in situ hybridization

3-µm FFPE sections were placed on electrostatically charged slides (Platinum Pro, Matsunami Glass Ind. Ltd, Japan). Fluorescence in situ hybridization (FISH) processing was done using the IntelliFISH Universal FFPE Tissue Pretreatment Kit (Vysis, Downer's Drove, IL, USA) according to the manufacturer's instructions and established laboratory protocol. The sections were then subjected to direct FISH using the 3p14.1, 6p22.1, and 6p22.3 probes (customized, Agilent, California, USA) (Table S6). Images were obtained using a Olympus BX61 microscope (Olympus Corporation, Tokyo, Japan) and captured on the Applied Image Analysis System v.3.93 (Applied Imaging, Pittsburgh, PA).

A total of 100 non-overlapping, intact interphase nuclei containing both red and green signals were enumerated. Green signal indicates the copy number of the target probes, while the red signal represents the copy number of the centromere control probes. A positive cell was defined as target signal number higher than 2, and more than the control signal number or equal to it. Amplification was determined by calculating the percentage of positive cells for 3p14.1, 6p22.1 and 6p22.3 probes with respect to the centromeric control probe. The cut-off for amplification was defined at 3 standard deviations (SD) above the mean of the FISH scores of 6 tonsil / lymph node control cases. A cut-off of 6.5% (mean=1.83, SD=1.46) was used for a positive result for the 3p14.1 probe, a cut-off of 6% (mean=2.13, SD=1.19) was used for the 6p22.1 probe, and a cut-off of 3% (mean=1.50, SD=0.35) was used for the 6p22.3 probe.

Mutational analysis Targeted Next Generation Sequencing

Targeted mutation analysis was performed by Next Generation Sequencing (Ion GeneStudio S5 prime, Thermo Fisher Scientific, Waltham, MA, USA) using an AmpliSeq Custom Panel designed for this study comprising a total of 35 genes commonly mutated in ENKTL and PTCL-NOS (Table S3A). Amplicon library preparation and semiconductor sequencing was done according to the manufacturers' manuals using the Ion AmpliSeq Library Kit v2.0, the Ion Library TaqMan Quantitation Kit, the Ion 510 & Ion 520 & Ion 530 Kit – Chef, the Ion 520 Chip Kit and the Ion 530 Chip Kit (Thermo Fisher Scientific).

Variant calling of non-synonymous somatic variants compared to the human reference sequence was performed using Ion Reporter Software (Thermo Fisher Scientific, Version 5.12.3.0). Variants were filtered with a threshold allele frequency of 5-10% (per sample panel optimized cutoff). Variants called by the Ion Reporter Software were visualized using the Integrative Genomics Viewer (IGV; Broad Institute, Cambridge, MA; Version 2.5.0 to Version 2.8.0) to exclude panel-specific artefacts.

Mutational analysis using Novogene Precision Medicine 2.0 (NovoPM™ 2.0)

Genomic variations in the 15 PTCL-EBV cases were screened using the 484-gene NovoPM™ 2.0 genomic profiling assay (Table S3B). Before reference genome alignment, low-quality reads (Phred quality score < 30) and reads containing adapters were removed to control data quality. Three cases with less than 90% coverage at 50x depth were excluded from further analysis. After the variant calling, all somatic variants with reported variant allele frequency (VAF) < 5%, were identified as possible artifacts and excluded. Mutation is reported when VAF≥5%. Finally, somatic variants that reported Exome Aggregation Consortium, in All populations (ExAC_ALL) > 1%, were also excluded from the analysis. The remaining 11 cases were subjected to Tumor Mutation Burden (TMB) and Microsatellite Instability (MSI) analysis. TMB was calculated based on the coding DNA sequence (CDS) regions included in the NovoPM™ 2.0 panel, approximately 1.4 MB. Synonymous mutations or functionally silent mutations were excluded from the TMB calculation.

Multiplexed immunofluorescence and multispectral imaging

Multiplex immunofluorescence (MIF) staining was performed to assess BIRC3, CD3, CD27 and P50 expression on 3-μm FFPE tissue sections using the Opal 7-color Flourophore TSA plus Fluorescence Kit (NEL 797001KT, Perkin Elmer). Slides were stained with CD3/CD27/P50/BIRC3/DAPI on Bond RX Biosystem (Leica, Wetzlar, Germany). Slides were deparaffinised in xylene and rehydrated in ethanol. Slides then underwent 4 rounds of sequential IF staining (Table S17). PD-L1/CD3 MIF staining procedures were described previously.[13]

The most representative tumor-rich regions pre-determined by an experienced hematopathologist were analyzed using InForm 2.4.8 image analysis software. Using Vectra 2 multispectral automated imaging system (Perkin Elmer), 20 to 30 images were scanned for whole tissue sections and 2-8 tissue microarray (TMA) cores were scanned for TMA cases at 20x magnification. On average, about 18,000 cells were scored and analyzed per case.

Cells were segmented based on nuclear counterstain DAPI using the inform 2.4.8 image analysis software. For every marker, including CD3, the fluorescent intensity cutoff value for positivity was decided by the pathologist according to the staining pattern and intensity on each selected image, with cross reference to simulated bright field images. Based on this cut-off, cells were scored by the InForm software as positive or negative for each marker. Similarly, using the positive cutoff for CD3, cells can be scored as positive (tumor cells) or negative (non-tumor cells). The following number of cases were quantified for each marker tested in the MIF panel: ENKTL (n=14), PTCL-EBV (n=13) and PTCL-NOS (n=13). We quantified the expression of BIRC3, CD27 and p50 in tumour (CD3+) and non-tumour cells (CD3-) and computed the expression of CD27+/p50+, CD27+/BIRC3+, BIRC3+/p50+, CD27+/p50+/BIRC3+ populations in tumour and non-tumour cells.

References

1. Pileri SA, Weisenburger DD, Sng I, Nakamura S, Muller-Hermelink hk, Chan WC, Jaffe ES. Peripheral T-cell lymphoma, NOS. In: Swerdlow SH, Campo E, Harris NL, et al., eds. WHO Classification of Tumours of Haematopoietic and Lymphoid Tissues. International Agency for Research on Cancer; 2017:403-407.

2. Ng S-B, Chung T-H, Kato S, Nakamura S, Takahashi E, Ko Y-H, et al. Epstein-Barr virus-associated primary nodal T/NK-cell lymphoma shows a distinct molecular signature and copy number changes. Haematologica. 2018 Feb;103(2):278–87.

3. Cheadle C, Vawter MP, Freed WJ, Becker KG. Analysis of microarray data using Z score transformation. J Mol Diagn. 2003 May;5(2):73–81.

4. Andor N, Graham TA, Jansen M, Xia LC, Aktipis CA, Petritsch C, et al. Pan-cancer analysis of the extent and consequences of intratumor heterogeneity. Nat Med. 2016 Jan;22(1):105–13.

5. Sinha S, Mitchell KA, Zingone A, Bowman E, Sinha N, Schäffer AA, et al. Higher prevalence of homologous recombination deficiency in tumors from African Americans versus European Americans. Nature Cancer. 2020 Jan 1;1(1):112–21.

6. EaCoN [Internet]. Github; [cited 2020 Oct 15]. Available from: https://github.com/gustaveroussy/EaCoN

7. Mermel CH, Schumacher SE, Hill B, Meyerson ML, Beroukhim R, Getz G. GISTIC2.0 facilitates sensitive and confident localization of the targets of focal somatic copy-number alteration in human cancers. Genome Biol. 2011;12(4):R41.

8. Subramanian A, Tamayo P, Mootha VK, Mukherjee S, Ebert BL, Gillette MA, et al. Gene set enrichment analysis: a knowledge-based approach for interpreting genome-wide expression profiles. Proc Natl Acad Sci U S A. 2005 Oct 25;102(43):15545–50.

9. Liberzon A, Subramanian A, Pinchback R, Thorvaldsdóttir H, Tamayo P, Mesirov JP. Molecular signatures database (MSigDB) 3.0. Bioinformatics. 2011 Jun 15;27(12):1739–40.

10. Newman AM, Steen CB, Liu CL, Gentles AJ, Chaudhuri AA, Scherer F, et al. Determining cell type abundance and expression from bulk tissues with digital cytometry. Nat Biotechnol. 2019 May 6;37(7):773–82.

11. Ng S-B, Selvarajan V, Huang G, Zhou J, Feldman AL, Law M, et al. Activated oncogenic pathways and therapeutic targets in extranodal nasal-type NK/T cell lymphoma revealed by gene expression profiling. J Pathol. 2011 Mar;223(4):496–510.

12. Qureshi A, Thakur N, Monga I, Thakur A, Kumar M. VIRmiRNA: a comprehensive resource for experimentally validated viral miRNAs and their targets. Database [Internet]. 2014 Nov 7;2014. Available from: http://dx.doi.org/10.1093/database/bau103

13. Hong G, Fan S, Phyu T, Maheshwari P, Hoppe MM, Phuong HM, et al. Multiplexed Fluorescent Immunohistochemical Staining, Imaging, and Analysis in Histological Samples of Lymphoma. J Vis Exp [Internet]. 2019 Jan 9;(143). Available from: http://dx.doi.org/10.3791/58711

Supplementary Tables

Supplemental Table 1. Comparison of diagnostic criteria between PTCL-EBV and ENKTL

	PTCL-EBV	*ENKTL*
Main (primary) tumor bulk and disease presentation	*Lymph node*	*Extranodal*
Nasal involvement	*No*	*Yes*
CD8	*+/-*	*-/+*
CD56	*-/+*	*+/-*
Lineage	*T >> NK*	*NK >> T*

Supplemental Table 2A and 2B. Summary of all cases (Refer to Supplemental Table 2A) and PTCL-EBV (Refer to Supplemental Table 2B.xls)

Supplementary Table 3A. AmpliSeq Custom Panel of known mutations in T/NK lymphoid panel

Gene symbol	Transcript	Position (GRCh37/hg19)	Exon(s)	Amplicon*
ARID1A	NM_006015	chr1:27,022,972 - chr1:27,107,247	CDS	80
ATM	NM_000051	chr11:108,098,352 - chr11:108,236,235	CDS	148
BCOR	NM_001123385	chrX:39,911,362 - chrX:39,937,182	CDS	65
CARD11	NM_032415	chr7:2,946,272 - chr7:2,998,140	CDS	54
CCR4	NM_005508	chr3:32,994,915 - chr3:32,995,997	CDS	11
CD28	NM_006139	chr2:204,571,420 - chr2:204,599,635	CDS	11
CD58	NM_001779	chr1:117,057,435 - chr1:117,113,594	CDS	13
CTNNB1	NM_001904	chr3:41,265,560 - chr3:41,280,833	CDS	32
DDX3X	NM_001356	chrX:41,193,506 - chrX:41,206,972	CDS	35
DMXL2	NM_001174116	chr15:51,741,181 - chr15:51,914,742	CDS	129
DNMT3A	NM_022552	chr2:25,457,148 - chr2:25,536,853	CDS	47
FYN	NM_153047	chr6:111,982,942 - chr6:112,041,254	CDS	29
IDH2	NM_002168	chr15:90,631,758 - chr15:90,631,957	Exon 4‡	2

IRF4	NM_002460	chr6:393,153 - chr6:407,598	CDS	18
JAK1	NM_002227	chr1:65,300,245 - chr1:65,351,947	CDS	56
JAK3	NM_000215	chr19:17,937,552 - chr19:17,955,226	CDS	52
KMT2D	NM_003482	chr12:49,415,563 - chr12:49,449,107	CDS	193
MGA	NM_001164273	chr15:41,961,093 - chr15:42,059,478	CDS	110
MSN	NM_002444	chrX:64,887,709 - chrX:64,959,755	CDS	24
NRAS	NM_002524	chr1:115,251,156 - chr1:115,258,781	CDS	9
PIK3CD	NM_005026	chr1:9,770,514 - chr1:9,787,104	CDS	47
PLCG1	NM_002660	chr20:39,766,358 - chr20:39,803,149	CDS	65
PRDM1	NM_001198	chr6:106,534,436 - chr6:106,555,361	CDS	29
PRKCB	NM_002738	chr16:24,183,570 - chr16:24,183,694	Exon 11[†]	1
PTPN1	NM_002827	chr20:49,127,065 - chr20:49,199,252	CDS	21
RHOA	NM_001664	chr3:49,412,916 - chr3:49,413,022	Exon 2[†]	1
SETD2	NM_014159	chr3:47,058,583 - chr3:47,205,358	CDS	91
STAT3	NM_139276	chr17:40,475,261 - chr17:40,475,385	Exon 19[†]	1
STAT3	NM_139276	chr17:40,474,964 - chr17:40,475,169	Exon 20[†]	2
STAT3	NM_139276	chr17:40,474,238 - chr17:40,474,522	Exon 21[†]	3
STAT3	NM_139276	chr17:40,469,155 - chr17:40,469,285	Exon 22[†]	1
STAT5B	NM_012448	chr17:40,362,340 - chr17:40,362,520	Exon 14[†]	2
STAT5B	NM_012448	chr17:40,362,101 - chr17:40,362,322	Exon 15[†]	2
STAT5B	NM_012448	chr17:40,359,505 - chr17:40,359,810	Exon 16[†]	3
STAT5B	NM_012448	chr17:40,354,707 - chr17:40,354,888	Exon 17[†]	2
STAT5B	NM_012448	chr17:40,354,362 - chr17:40,354,475	Exon 18[‡]	1
TET2	NM_001127208	chr4:106,155,100 - chr4:106,197,676	CDS	67
TNFAIP3	NM_001270507	chr6:138,192,365 - chr6:138,202,456	CDS	29
TNFRSF1B	NM_001066	chr1:12,227,149 - chr1:12,267,077	CDS	22
TP53	NM_000546	chr17:7,572,927 - chr17:7,579,912	CDS	22
VAV1	NM_001258207	chr19:6,772,819 - chr19:6,857,118	CDS	45

*Amplicon length:125-175bp; [†]Exon completely covered; [‡]Exon not completely covered; CDS, coding sequence.

Supplementary Table 3B. List of genes investigated using Novogene Precision Medicine 2.0 (NovoPM^{TM}) Panel

SNV | InDel | CNV						
ABCB1	ABCC2	ABCC4	ABCG2	ABL1	ABL2	ABRAXAS1
ACVR1B	ADGRA2	AKT1	AKT2	AKT3	ALK	ALOX12B
AMER1	APC	APCDD1	AR	ARAF	ARFRP1	ARID1A
ARID1B	ARID2	ASXL1	ATM	ATR	ATRX	AURKA
AURKB	AXIN1	AXIN2	AXL	BACH1	BAP1	BARD1
BCL2	BCL2A1	BCL2L1	BCL2L2	BCL6	BCOR	BCORL1
BCR	BLM	BMPR1A	BRAF	BRCA1	BRCA2	BRD4
BRIP1	BTG1	BTG2	BTK	C8orf34	CALR	CARD11
CASP8	CBFB	CBL	CCND1	CCND2	CCND3	CCNE1
CD22	CD274	CD70	CD74	CD79A	CD79B	CDC73
CDH1	CDH2	CDH20	CDH5	CDK12	CDK4	CDK6
CDK8	CDKN1A	CDKN1B	CDKN2A	CDKN2B	CDKN2C	CEBPA
CFTR	CHD2	CHD4	CHEK1	CHEK2	CHUK	CIC
CRBN	CREBBP	CRKL	CRLF2	CSF1R	CSF3R	CTCF
CTNNA1	CTNNB1	CUL3	CUL4A	CUL4B	CXCR4	CYLD
CYP17A1	CYP1B1	CYP2C19	CYP2C8	CYP2D6	CYP3A4	CYP3A5
DAXX	DDR1	DDR2	DICER1	DIS3	DNMT3A	DOT1L
DPYD	EED	EGFR	EMSY	EP300	EPCAM	EPHA3
EPHA5	EPHA6	EPHA7	EPHB1	EPHB4	EPHB6	ERBB2
ERBB3	ERBB4	ERCC1	ERCC2	ERCC3	ERCC4	ERG
ERRFI1	ESR1	ESR2	ETV1	ETV4	ETV5	ETV6
EWSR1	EZH2	EZR	FAM46C	FANCA	FANCC	FANCD2
FANCE	FANCF	FANCG	FANCI	FANCL	FANCM	FAS
FAT1	FAT3	FBXW7	FCGR3A	FGF10	FGF12	FGF14
FGF19	FGF23	FGF3	FGF4	FGF6	FGF7	FGFR1
FGFR2	FGFR3	FGFR4	FH	FLCN	FLT1	FLT3
FLT4	FOXL2	FOXP1	FRS2	FUBP1	GABRA6	GALNT12

GATA1	GATA2	GATA3	GATA4	GATA6	GEN1	GID4
GLI1	GNA11	GNA13	GNAQ	GNAS	GREM1	GRIN2A
GRM3	GSK3B	GSTP1	H3F3A	HDAC1	HDAC2	HFE
HGF	HLA-A	HLA-B	HLA-C	HNF1A	HOXB13	HRAS
HSD3B1	HSP90AA1	ID3	IDH1	IDH2	IDO1	IDO2
IGF1	IGF1R	IGF2	IGF2R	IKBKE	IKZF1	IL7R
INHBA	INPP4B	INSR	IRF2	IRF4	IRS2	ITPA
JAK1	JAK2	JAK3	JUN	KAT6A	KDM5A	KDM5C
KDM6A	KDR	KEAP1	KEL	KIT	KLHL6	KMT2A
KMT2C	KMT2D	KRAS	LMO1	LRP1B	LRP2	LRP6
LTK	LYN	LZTR1	MAF	MAGI2	MAN1B1	MAP2K1
MAP2K2	MAP2K4	MAP3K1	MAP3K13	MAPK1	MAX	MC1R
MCL1	MDM2	MDM4	MED12	MEF2B	MEN1	MERTK
MET	MITF	MKNK1	MKNK2	MLH1	MLH3	MPL
MRE11	MSH2	MSH3	MSH6	MST1R	MTAP	MTHFR
MTOR	MUTYH	MYB	MYC	MYCL	MYCN	MYD88
NBN	NCOR1	NF1	NF2	NFE2L2	NFKBIA	NKX2-1
NOTCH1	NOTCH2	NOTCH3	NOTCH4	NPM1	NQO1	NRAS
NRP2	NSD1	NSD2	NSD3	NT5C2	NTHL1	NTRK1
NTRK2	NTRK3	NUDT1	NUP93	NUTM1	P2RY8	PAK3
PAK5	PALB2	PARP1	PARP2	PARP3	PARP4	PAX5
PBRM1	PDCD1	PDCD1LG2	PDGFRA	PDGFRB	PDK1	PHLPP2
PIK3C2B	PIK3C2G	PIK3C3	PIK3CA	PIK3CB	PIK3CG	PIK3R1
PIK3R2	PIM1	PLCG2	PMS2	PNRC1	POLD1	POLE
PPARG	PPM1D	PPP2R1A	PPP2R2A	PRDM1	PREX2	PRKAR1A
PRKCI	PRKDC	PRKN	PRSS1	PRSS8	PTCH1	PTCH2
PTEN	PTPN11	PTPRD	PTPRO	QKI	RAC1	RAD21
RAD50	RAD51	RAD51B	RAD51C	RAD51D	RAD52	RAD54L
RAF1	RANBP2	RARA	RB1	RBM10	REL	RET
RICTOR	RNF43	ROS1	RPA1	RPTOR	RSPO2	RUNX1

RUNX1T1	SDC4	SDHA	SDHAF2	SDHB	SDHC	SDHD
SETD2	SF3B1	SGK1	SH2B3	SLC19A1	SLC22A2	SLC34A2
SLCO1B3	SLIT2	SMAD2	SMAD3	SMAD4	SMARCA4	SMARCB1
SMARCD1	SMO	SNCAIP	SOCS1	SOD2	SOX10	SOX2
SOX9	SPEN	SPINK1	SPOP	SPTA1	SRC	STAG2
STAT3	STAT4	STK11	SUFU	SULT1A1	SYK	TAF1
TBX3	TDO2	TEK	TERC	TERT	TET2	TGFBR2
TIPARP	TMEM127	TMPRSS2	TNF	TNFAIP3	TNFRSF14	TNKS
TNKS2	TOP1	TOP2A	TP53	TP53BP1	TPMT	TRRAP
TSC1	TSC2	TSHR	TYMS	TYRO3	U2AF1	UGT1A1
UMPS	VEGFA	VHL	WISP3	WRN	WT1	XPC
XPO1	XRCC1	XRCC2	XRCC3	ZBTB2	ZNF217	ZNF703
ZNRF3						

SNV, Single Nucleotide Variant; INDEL, Insertion/Deletion; CNV, Copy Number Variation.

Supplementary Table 4. Recurrent copy number gains in ENKTL, PTCL-EBV and PTCL-NOS groups

Cytoband	Outputs of GISTIC2				Comparison of CNV status						
	Q value	Peak boundaries	No. of target genes	Target Genes	ENKTL (n)	PTCL-EBV (n)	PTCL-NOS (n)	ENKTL (%frequency)	PTCL-EBV (%frequency)	PTCL-NOS (%frequency)	P (Chi-squared test)
1p13.3	0.035	chr1:110210672-110246358	2	GSTM1,GSTM2	3	1	6	8.82	7.14	20.69	0.342
2q33.2	0.114	chr2:200091395-205385453	11	CD28,CTLA4,ABI2,ICOS,WDR12,CYP20A1, RAPH1,NBEAL1,ALS2CR8,ICA1L,FAM117B	3	1	7	8.82	7.14	24.14	0.204
3p14.1	0.000	chr3:67756118-68071040	1	FAM19A1	2	2	22	5.88	14.29	75.86	4.500E-06
6p22.3	0.011	chr6:21578113-21677059	2	SOX4,LINC00340	7	1	17	20.59	7.14	58.62	5.640E-03
6p22.1	0.027	chr6:27041283-27128306	7	hsa-mir-3143,HIST1H4I,HIST1H2AG,HIST1H2BJ,HIST1H2AH,HIST1H2BK,MIR3143	3	3	17	8.82	21.43	58.62	1.230E-03
6p21.32	0.114	chr6:32441009-32600525	3	HLA-DRB1,HLA-DRB5,HLA-DRB6	5	2	7	14.71	14.29	24.14	0.634
8q24.21	0.041	chr8:128939865-129031733	5	hsa-mir-1206,hsa-mir-1205,PVT1,MIR1205,MIR1206	11	1	10	32.35	7.14	34.48	0.249
9p24.1	0.114	chr9:5094540-5830316	10	INSL4,JAK2,RLN1,RLN2,INSL6,CD274,C9orf46,KIAA1432,ERMP1,PDCD1LG2	3	0	1	8.82	0.00	3.45	0.414
14q32.33	0.222	chr14:106634418-106770053	1	LINC00226	8	3	11	23.53	21.43	37.93	0.486
17q21.33	0.037	chr17:47484004-47761681	4	NGFR,PHB,SPOP,NXPH3	8	0	13	23.53	0.00	44.83	0.026
22q11.23	0.114	chr22:24338652-24402275	4	GSTT1,GSTTP1,LOC391322,GSTTP2	3	2	5	8.82	14.29	17.24	0.645

Supplementary Table 5. Recurrent copy number losses in ENKTL, PTCL-EBV and PTCL-NOS groups

Cytoband	Outputs of GISTIC2				Comparison of CNV status						
	Q value	Peak boundaries	No. of target genes	Target Genes	ENKTL (n)	PTCL-EBV (n)	PTCL-NOS (n)	ENKTL (%frequency)	PTCL-EBV (%frequency)	PTCL-NOS (%frequency)	P (Chi-squared test)
3q26.1	1.200E-27	chr3:162440046-162619269	1	LOC647107	17	8	14	50.00	57.14	48.28	0.927
6q24.3	0.004	chr6:130791690-162850142	12	GRM1,EPM2A,RAB32,SASH1,ADGB,FBXO30,STXBP5,SHPRH,SAMD5,LOC729176,LOC729178,LOC100507557	14	2	5	41.18	14.29	17.24	0.114
8p22	0.106	chr8:15057079-16147734	18	hsa-mir-548v,hsa-mir-383,MSR1,PDGFRL,SLC7A2,TUSC3,MTMR7,DLC1,FGF20,CNOT7,ZDHHC2,MTUS1,KIAA1456,VPS37A,SGCZ,C8orf48,EFHA2,MIR383	5	2	2	14.71	14.29	6.90	0.633
9p21.3	4.956E-10	chr9:21992224-22014523	4	CDKN2A,CDKN2B,CDKN2B-AS1,C9orf53	6	1	8	17.65	7.14	27.59	0.344
14q11.2	1.859E-50	chr14:22713427-22751112	1	DAD1	7	14	17	20.59	100.00	58.62	1.100 E-03
17p13.1	0.044	chr17:7533556-7598662	138	hsa-mir-4314,hsa-mir-324,hsa-mir-497, ACADVL,ALOX12,ALOX12B,ALOX12P2,ALOX15B,ASGR1,ASGR2,ATP1B2,CD68,CHD3,CHRNB1,CLDN7,DLG4,DVL2,EFNB3,EIF4A1,EIF5A,FGF11,GPS2,GUCY2D,MYH1,MYH2,MYH3,MYH4,MYH8,MYH10,PER1,PFAS,POLR2A,RCVRN,RPL26,SCO1,SHBG,SLC2A4,SOX15,VAMP2,TP53,GAS7,TNK1,MYH13,TNFSF13,TNFSF12,KCNAB3,AURKB,GLP2R,NTN1,STX8,FXR2,MPDU1,ACAP1,CLEC10A,GABARAP,ARHGEF15,KDM6B,CTDNEP1,PIK3R5,C17orf81,SENP3,SNORA67,RANGRF,MED31,YBX2,XAF1,C17orf59,WRAP53,C17orf48,PLSCR3,NLGN2,ZBTB4,TRAPPC1,ALOXE3,PHF23,CTC1,NDEL1,TEKT1,TMEM107,LSMD1,NEURL4,HES7,TXNDC17,TMEM88,SAT2,CNTROB,RPL29P2,CYB5D1,USP43,KRBA2,C17orf49,DNAH2,WDR16,CCDC42,PIK3R6,ODF4,KCTD11,MFSD6L,SLC16A11,FBXO39,DHRS7C,SLC16A13,C17orf74,C17orf61,B	9	1	9	26.47	7.14	31.03	0.322

				CL6B,LOC284023,LINC00324,SLC13A5,TMEM102,TMEM95,ALOX15P1,SPEM1,C17orf100,SPDYE4,TMEM220,SLC25A35,MIR195,TNFSF12-TNFSF13,RNASEK,MIR324,MIR497,SLC35G6,RNF222,SNORA48,SNORD10,SCARNA21,LOC100128288,LOC100289255,MIR4314,MIR3676,LOC100506713,MIR497HG,RNASEK-C17ORF49,C17orf61-PLSCR3,SENP3-EIF4A1,MIR4520A,MIR4521,MIR4520B							
18q22.3	0.232	chr18:68144384-69233856	1	LOC100505776	5	0	7	14.71	0.00	24.14	0.169
19p13.3	0.096	chr19:1-422937	68	hsa-mir-3187,hsa-mir-1302-11,ATP5D,AZU1,HCN2,BSG,CDC34,CIRBP,CNN2,CFD,ARID3A,EFNA2,ELANE,GAMT,GPX4,GZMM,PALM,POLR2E,POLRMT,PRTN3,PTBP1,RPS15,STK11,TCF3,MADCAM1,PPAP2C,MED16,FSTL3,APC2,ABCA7,UQCR11,SBNO2,SHC2,DAZAP1,FGF22,THEG,MBD3,MIER2,PCSK4,C19orf24,RNF126,WDR18,LPPR3,OR4F17,KISS1R,MUM1,MIDN,R3HDM4,C19orf6,TPGS1,REEP6,GRIN3B,C19orf21,PLK5,C2CD4C,CIRBP-AS1,C19orf25,C19orf26,ODF3L2,ADAMTSL5,NDUFS7,WASH5P,MEX3D,FLJ45445,PRSS57,MIR3187,MIR4745	3	0	6	8.82	0.00	20.69	0.143
22q11.23	8.994E-53	chr22:24361439-24382737	2	GSTT1,LOC391322	23	6	8	67.65	42.86	27.59	0.069

Supplementary Table 6. Fluorescence in situ hybridization of top two recurrent copy number gains among three disease groups

A

Probe	Target Region	Size (kbp)
3p14.1	chr3:67767481-68054390	286.91
6p22.1	chr6:26986146-27136475	150.33

B

Probe			Oncoscan results		
			Negative	Positive	Total
3p14.1	FISH results	Negative	4	3	7
		Positive	2	15	17
		Total	6	18	24
6p22.1	FISH results	Negative	10	5	15
		Positive	1	7	8
		Total	11	12	23

C

Probe	Fisher's Exact test	Kappa test	
	P value	Kappa value	P value
3p14.1	0.038	0.474	0.020
6p22.1	0.027	0.485	0.013

(A) Target region and size of each probe used in FISH. (B) 15 out of 24 cases showed amplification for 3p14.1 probe and 7 out of 23 cases showed amplification for 6p22.1 probe. (C) Statistical test to determine significant association between FISH results and Oncoscan results for 3p14.1 and 6p22.1 probes (P=0.038 and 0.027 respectively). There was also moderate agreement between FISH results and Oncoscan data for 3p14.1 probe ($P = 0.020$) and 6p22.1 probe ($P = 0.013$).

Supplementary Table 7. Public Oncoscan datasets with details of disease types and accession numbers from GEO

Series	Ref	Abbreviation	Disease Type	n
GSE77571	*NA*	CML	Chronic Myeloid Leukemia	39
GSE116526	PMID:30733272	BL Lymphoma	Burkitt-like lymphoma	8
GSE128215	doi.org/10.1182/blood-2018-99-114493	LBC Lymphoma	Large B-Cell Lymphomas	51
GSE78872	PMID:27257180	pFL	Pediatric-type Follicular Lymphoma	34
GSE127231	*NA*	HNSCC	Head and neck squamous cell carcinoma	35
GSE107225	PMID:29203589	LNMCC	Lymph Node Metastases in Colon Cancer	33
GSE76014	PMID:27461516	OTC	oral tongue carcinoma	40
GSE85970	PMID:27713405	RCC	Renal cell carcinoma with unclassified histology	15
GSE73365	PMID:26568296	Rectal Cancer	Rectal Cancer	15
GSE110026	PMID:30151896	SCC	Synchronous colorectal cancer	106
GSE83916	PMID:28770103	Breast Cancer	Breast Cancer	26
GSE78926	PMID:27974698	ESCC	Esophageal Squamous Cell Carcinoma	38
GSE119042	PMID:30617134	Uterine Sarcoma	Uterine Sarcoma	40
GSE125255	PMID:32355162	Glioblastoma	Glioblastoma	56

NA, citation not available on GEO

Supplemental Table 8. Differentially expressed genes among the three disease groups (Refer to Supplemental Table 8.xls)

Supplementary Table 9A. Biological processes enriched for genes differentially expressed between ENKTL and PTCL-EBV.

Term ID	Term description	Observed	Background	FDR
GO:0002682	regulation of immune system process	39	1391	0.0052
GO:0002250	adaptive immune response	15	280	0.0059
GO:0002376	immune system process	51	2370	0.0368
GO:0002764	immune response-regulating signaling pathway	15	365	0.0368
GO:0006955	immune response	38	1560	0.0368
GO:0045619	regulation of lymphocyte differentiation	10	158	0.0368
GO:0050851	antigen receptor-mediated signaling pathway	9	122	0.0368
GO:0050852	T cell receptor signaling pathway	8	93	0.0368
GO:0050776	regulation of immune response	25	873	0.0379
GO:0045058	T cell selection	5	37	0.0451
GO:1902105	regulation of leukocyte differentiation	12	261	0.0451
GO:1903707	negative regulation of hemopoiesis	9	148	0.0451

FDR:false discovery rate

For each biological process identified, the corresponding Gene Ontology (GO) pathway and the

FDR are reported in the table.

Supplementary Table 9B. Cellular processes enriched for genes differentially expressed between ENKTL and PTCL-EBV.

Term ID	Term description	Observed	Background	FDR
GO:0043235	receptor complex	16	305	0.00093
GO:0005576	extracellular region	53	2505	0.01
GO:0005887	integral component of plasma membrane	38	1564	0.01
GO:0042101	T cell receptor complex	4	13	0.01
GO:0005615	extracellular space	29	1134	0.0138
GO:0044421	extracellular region part	33	1375	0.0138
GO:0098802	plasma membrane receptor complex	9	158	0.0138
GO:0009897	external side of plasma membrane	10	223	0.0289

FDR:false discovery rate

Supplementary Table 10. Biological processes enriched for genes differentially expressed between PTCL-EBV and PTCL-NOS.

Term ID	Term description	Observed	Background	FDR
GO:0006955	immune response	21	1560	0.0231
GO:0002250	adaptive immune response	8	280	0.0311
GO:0002376	immune system process	25	2370	0.0311
GO:0002449	lymphocyte mediated immunity	6	127	0.0311
GO:0002460	adaptive immune response based on somatic recombination of immune receptors built from immunoglobulin superfamily domains	6	132	0.0311
GO:0016064	immunoglobulin mediated immune response	5	72	0.0311
GO:1903707	negative regulation of hemopoiesis	6	148	0.0311
GO:1903706	regulation of hemopoiesis	9	412	0.0368
GO:2001183	negative regulation of interleukin-12 secretion	2	3	0.0425
GO:1902105	regulation of leukocyte differentiation	7	261	0.0498

FDR:false discovery rate

Supplementary Table 11. Top 10 hallmark gene sets from GSEA analysis.

Term	NES	FDR
HALLMARK_INTERFERON_ALPHA_RESPONSE	-3.251	0
HALLMARK_INTERFERON_GAMMA_RESPONSE	-3.130	2.097E-05
HALLMARK_IL6_JAK_STAT3_SIGNALING	-2.819	0.00103
HALLMARK_OXIDATIVE_PHOSPHORYLATION	-2.680	0.00206
HALLMARK_PROTEIN_SECRETION	-2.594	0.00350
HALLMARK_ALLOGRAFT_REJECTION	-2.544	0.00395
HALLMARK_TGF_BETA_SIGNALING	-2.548	0.00413
HALLMARK_TNFA_SIGNALING_VIA_ NFκB	-2.555	0.00414
HALLMARK_MYC_TARGETS_V1	-2.532	0.00419
HALLMARK_UNFOLDED_PROTEIN_RESPONSE	-2.507	0.00488

NES:normalized enrichment score; FDR:false discovery rate.

Supplemental Table 12. EBV gene expression and latency pattern determined by RT-PCR in ENKTL and PTCL-EBV cases

Disease	Study ID	EBNA-1	LMP-1	LMP-2A	EBNA-2	Latency
ENKTL	ENKTL04	+	+	+	-	2
ENKTL	ENKTL08	+	+	+	-	2
ENKTL	ENKTL30	+	+	+	-	2
ENKTL	ENKTL42	+/-	+	+	-	2
ENKTL	ENKTL61	+	+	+	+	3
ENKTL	ENKTL84	+	+	+	-	2
EBV+ PTCL	PTCL-EBV01	+	+	+	-	2
EBV+ PTCL	PTCL-EBV02	+	+	+	-	2
EBV+ PTCL	PTCL-EBV03	+	+	+	-	2
EBV+ PTCL	PTCL-EBV04	+	+	+	-	2
EBV+ PTCL	PTCL-EBV05	+	+	+	-	2
EBV+ PTCL	PTCL-EBV08	+	+	+	-	2
EBV+ PTCL	PTCL-EBV10	+	+	+	-	2
EBV+ PTCL	PTCL-EBV11	+	+	+	-	2
EBV+ PTCL	PTCL-EBV12	+	+	+	+/-	favour 3
EBV+ PTCL	PTCL-EBV13	+	+	+	+	3
EBV+ PTCL	PTCL-EBV14	+/-	+	+	+	favour 3
EBV+ PTCL	PTCL-EBV18	+	+	+	+	3
EBV+ PTCL	PTCL-EBV24	+	+	+	-	2

+, positive; -, negative; +/-, weakly positive.

Supplementary Table 13. Differential expression of EBV miRNA measured using qPCR

miRNA	Mean Ct difference	t	df	Adjust. *P*
ebv-miR-BART20-3p	3.979	5.061	19.835	0.003
ebv-miR-BART3-3p	6.933	4.331	13.250	0.005
ebv-miR-BART4-5p	5.721	4.588	15.435	0.005
ebv-miR-BART12	3.887	4.161	20.194	0.005
ebv-miR-BART16	4.962	3.936	20.768	0.005
ebv-miR-BART4-3p	5.699	4.225	16.489	0.005
ebv-miR-BART20-5p	3.898	4.061	19.686	0.005
ebv-miR-BART14-5p	3.658	3.837	20.224	0.005
ebv-miR-BART13-3p	4.106	3.737	18.870	0.006
ebv-miR-BART5-3p	3.926	3.719	20.019	0.006
ebv-miR-BART3-5p	5.397	3.728	16.234	0.007
ebv-miR-BART2-5p	4.651	3.494	18.885	0.009
ebv-miR-BART5-5p	5.399	3.525	15.334	0.009
ebv-miR-BART2-3p	3.351	3.393	20.354	0.009
ebv-miR-BART17-3p	5.013	3.309	18.386	0.010
ebv-miR-BART19-3p	5.397	3.324	17.593	0.010
ebv-miR-BART1-5p	6.217	3.527	13.430	0.010
ebv-miR-BART19-5p	3.808	3.300	16.089	0.010
ebv-miR-BART1-3p	6.717	3.341	12.233	0.013
ebv-miR-BART6-3p	6.178	3.144	13.915	0.015
ebv-miR-BART11-3p	3.822	2.852	20.885	0.018
ebv-miR-BART15	5.131	3.038	13.057	0.018
ebv-miR-BART17-5p	4.353	2.627	19.064	0.030
ebv-miR-BART6-5p	5.153	2.699	13.739	0.031
ebv-miR-BART7-3p	4.346	2.405	19.743	0.037
ebv-miR-BART14-3p	1.351	2.410	20.683	0.037

ebv-miR-BART21-3p	3.156	2.387	20.967	0.037
ebv-miR-BART18-3p	2.906	2.408	20.764	0.037
ebv-miR-BART9-5p	2.819	2.413	20.917	0.037
ebv-miR-BART7-5p	2.602	2.380	20.882	0.037
ebv-miR-BHRF1-2-3p	2.481	2.416	19.973	0.037
ebv-miR-BART10-3p	3.868	2.326	19.463	0.041
ebv-miR-BART9-3p	3.338	2.193	19.346	0.052
ebv-miR-BART8-5p	3.041	2.093	20.613	0.060
ebv-miR-BART10-5p	2.620	2.090	19.250	0.060
ebv-miR-BHRF1-2-5p	1.705	2.087	14.288	0.064
ebv-miR-BART18-5p	3.031	1.725	18.888	0.114
ebv-miR-BART22	3.036	1.657	20.230	0.125
ebv-miR-BHRF1-3	1.524	1.588	16.197	0.142
ebv-miR-BART11-5p	2.321	1.542	20.976	0.145
ebv-miR-BART8-3p	2.777	1.444	18.786	0.169
ebv-miR-BART21-5p	2.507	1.391	16.778	0.182

Mean Ct difference, [ENKTL mean Ct – PTCL-EBV mean Ct]; t, t-test statistic value; df, degree of freedom; Adjust.*P,* adjusted *P* value.

Supplementary Table 14. Differentially expressed EBV miRNA between ENKTL and PTCL-EBV and their target genes (Refer to Supplementary Table 14.xls)

Supplementary Table 15. Summary of Reactome pathways enriched for target genes of differentially expressed EBV miRNA (refer Supplementary Table 13)

Term ID	Term description	Observed	Background	FDR
HSA-168256	Immune System	41	1925	1.08E-05
HSA-1280215	Cytokine Signaling in Immune system	19	654	0.00095
HSA-913531	Interferon Signaling	10	189	0.0013
HSA-877300	Interferon gamma signaling	7	86	0.0018
HSA-168249	Innate Immune System	21	1012	0.0152
HSA-5653656	Vesicle-mediated transport	16	649	0.0152
HSA-74160	Gene expression (Transcription)	25	1366	0.0166
HSA-199991	Membrane Trafficking	15	612	0.0167
HSA-3247509	Chromatin modifying enzymes	9	238	0.0167
HSA-1839117	Signaling by cytosolic FGFR1 fusion mutants	3	16	0.0269
HSA-195258	RHO GTPase Effectors	9	273	0.0292
HSA-6807004	Negative regulation of MET activity	3	20	0.0406
HSA-5663202	Diseases of signal transduction	10	360	0.0451
HSA-982772	Growth hormone receptor signaling	3	22	0.0452

Supplemental Table 16. Multivariate analysis for overall survival across ENKTL, PTCL-EBV, cytotoxic PTCL-NOS and non-cytotoxic PTCL-NOS groups.

Variable	Category	Multivariate Analysis		
		HR	CI (95%)	P
Disease Type	ENKTL	0.65	0.34-1.26	0.2
	PTCL-EBV	1	Ref	
	Cytotoxic PTCL-NOS	0.22	0.08-0.58	0.002
	Non-cytotoxic PTCL-NOS	0.47	0.18-1.24	0.13
Stage	1	1	Ref	
	2	1.51	0.62-3.70	0.4
	3	1.47	0.48-4.52	0.5
	4	4.58	2.44-8.59	<0.001
Sex	Female	1	Ref	
	Male	1.38	0.84-2.39	0.2
Age		1.03	1.01-1.04	0.006

Supplementary Table 17. Multiplexed immunofluorescence staining procedures

Procedures		Reagent (dilution, product number, company)	Duration (min)	Temp (°C)
1st round	Antigen retrieval	ER1 (ready-to-use, AR9961, Leica)	20	100
	Epitope blocking	Blocking buffer (ready-to-use, ADR1001EA, Perkin Elmer)	10	RT
	Antibody incubation	anti-CD27 (1:100, ab1312541, Abcam)	60	RT
	Secondary antibody incubation	anti-Rabbit polymer (ready-to-use, K4003, DAKO)	30	RT
	Signal amplification and fluorophore deposition	Opal 520 (1:100, FP1487001KT, Perkin Elmer)	10	RT
2nd round	Antigen retrieval (antibody stripping)	ER1 (ready-to-use, AR9961, Leica)	20	100
	Epitope blocking	Blocking buffer (ready-to-use, ADR1001EA, Perkin Elmer)	10	RT
	Antibody incubation	anti-NFkB p50 (1:50, sc-8414, Santa Cruz)	60	RT
	Secondary antibody incubation	anti-Mouse polymer (ready-to-use, K4001, DAKO)	90	RT
	Signal amplification and fluorophore deposition	Opal 540 (1:100, FP1494001KT, Perkin Elmer)	10	RT
3rd round	Antigen retrieval (antibody stripping)	ER1 (ready-to-use, AR9961, Leica)	20	100
	Epitope blocking	Blocking buffer (ready-to-use, ADR1001EA, Perkin Elmer)	10	RT
	Antibody incubation	anti-BIRC3 (1:100, ab32059, Abcam)	15	RT
	Secondary antibody incubation	post primary and polymer (ready-to-use, DS9800, Leica)	8 each	RT
	Signal amplification and fluorophore deposition	Opal 620 (1:100, FP1495001KT, Perkin Elmer)	10	RT
4th round	Antigen retrieval (antibody stripping)	ER1 (ready-to-use, AR9961, Leica)	20	100
	Epitope blocking	Blocking buffer (ready-to-use, ADR1001EA, Perkin Elmer)	10	RT
	Antibody incubation	anti-CD3 (1:100, A0452, DAKO)	60	RT
	Secondary antibody incubation	anti-Rabbit polymer (ready-to-use, K4003, DAKO)	10	RT

	Signal amplification and fluorophore deposition	Opal 690 (1:100, FP1497001KT, Perkin Elmer)	10	RT
	Antibody stripping	ER1 (ready-to-use, AR9961, Leica)	20	100
	Counterstain	DAPI (1:50, FP1490, Perkin Elmer)	5	RT
	Mounting	CC mount (ready-to-use, C9368, Sigma)	-	RT

Temp, temperature; RT, room temperature

Supplementary Figures
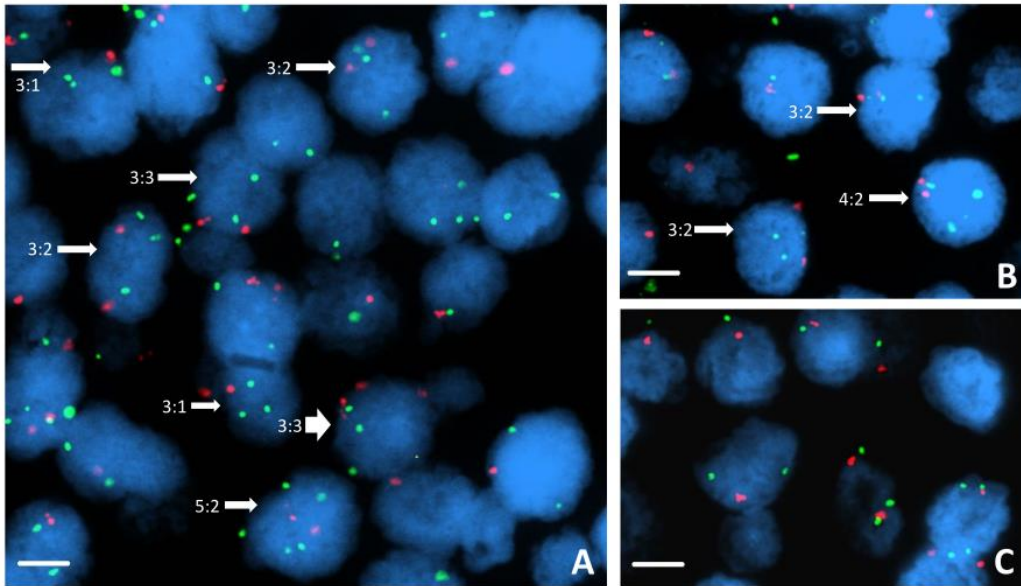
Supplementary Figure 1. Validation of top two recurrent copy-number gains using Fluorescence in situ hybridization. Representative images showing copy number gain (amplification) of (A) 3p14.1 probe and (B) 6p22.1. Green signal indicates target probe while red signal represents the centromere control probe. White arrows highlight cells with more green signals than red signals (target probe: centromere control). Arrowhead indicates cells with equal numbers of red and green signals. (C) Negative control for 3p14.1 probe showing cells without gain of 3p14.1. Scale bars represent 30μm.
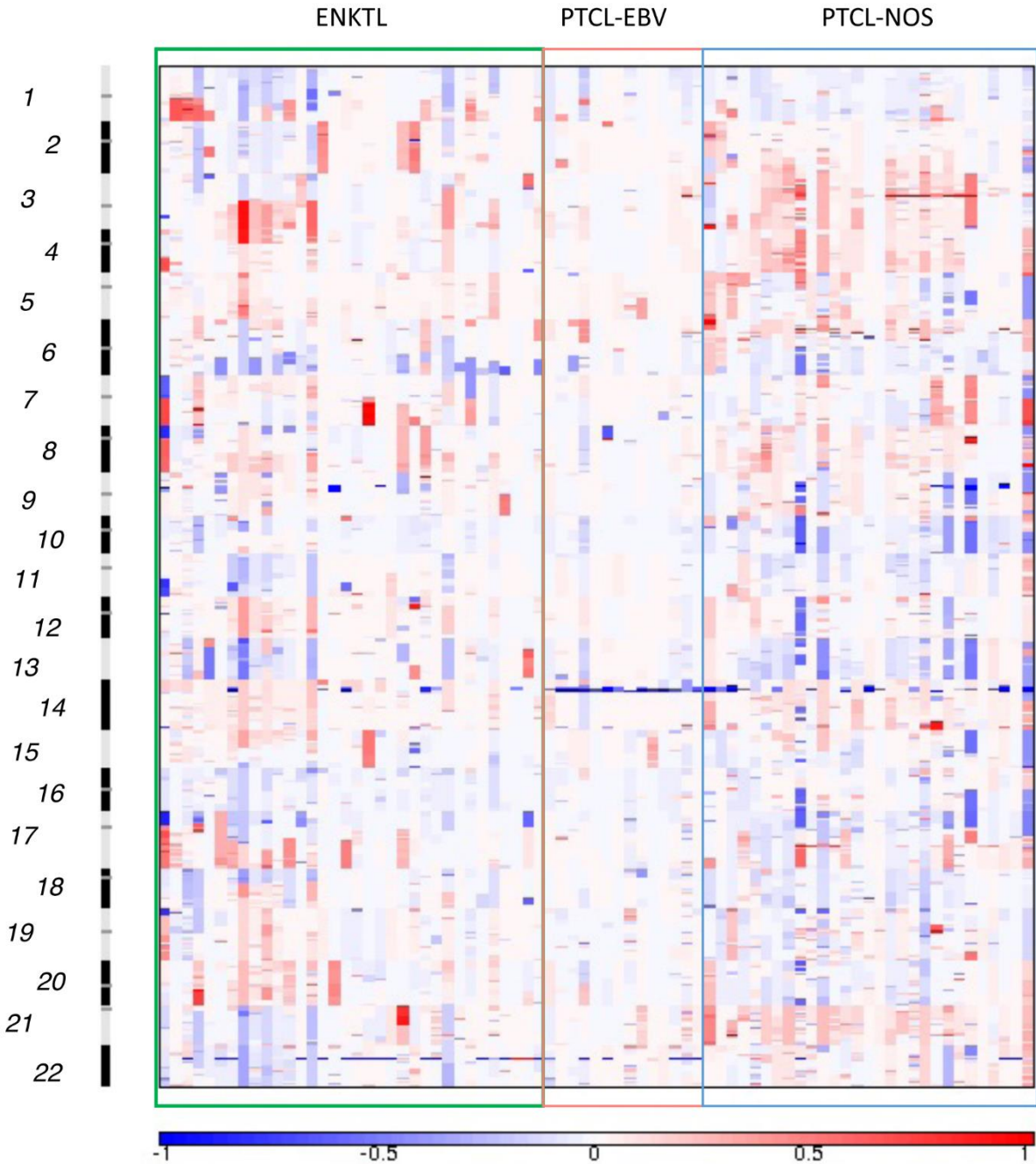
Supplementary Figure 2. Composite maps comparing genome-wide CNA across all three diseases. Gains are represented in red and losses in blue. Our results showed that PTCL-EBV exhibited fewer and less frequent genomic alterations compared to ENKTL and PTCL-NOS.
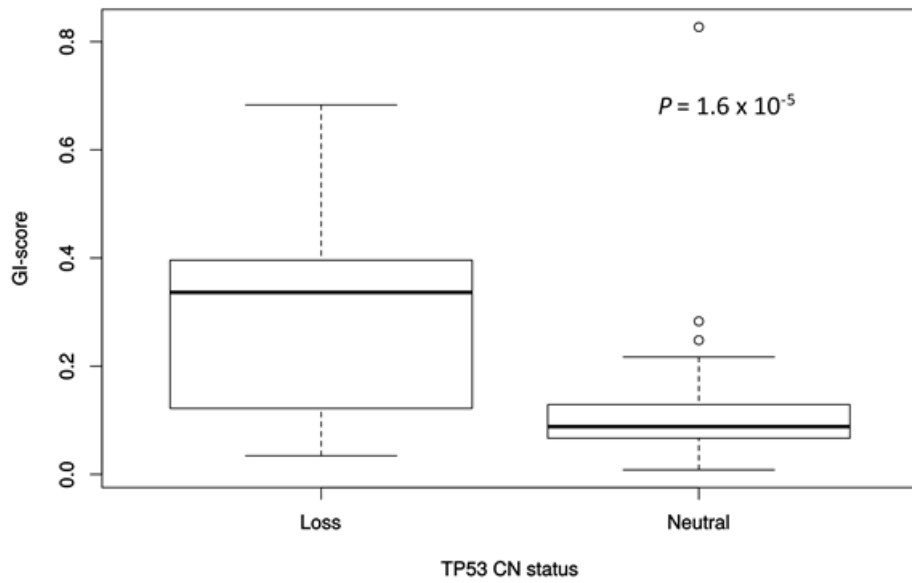
Supplementary Figure 3. Association of GI score with TP53 copy- number status across three diseases. Comparison of GI score between cases with or without TP53 copy number loss across all three disease groups. Results showed significantly higher GI score in cases with *TP53* loss.
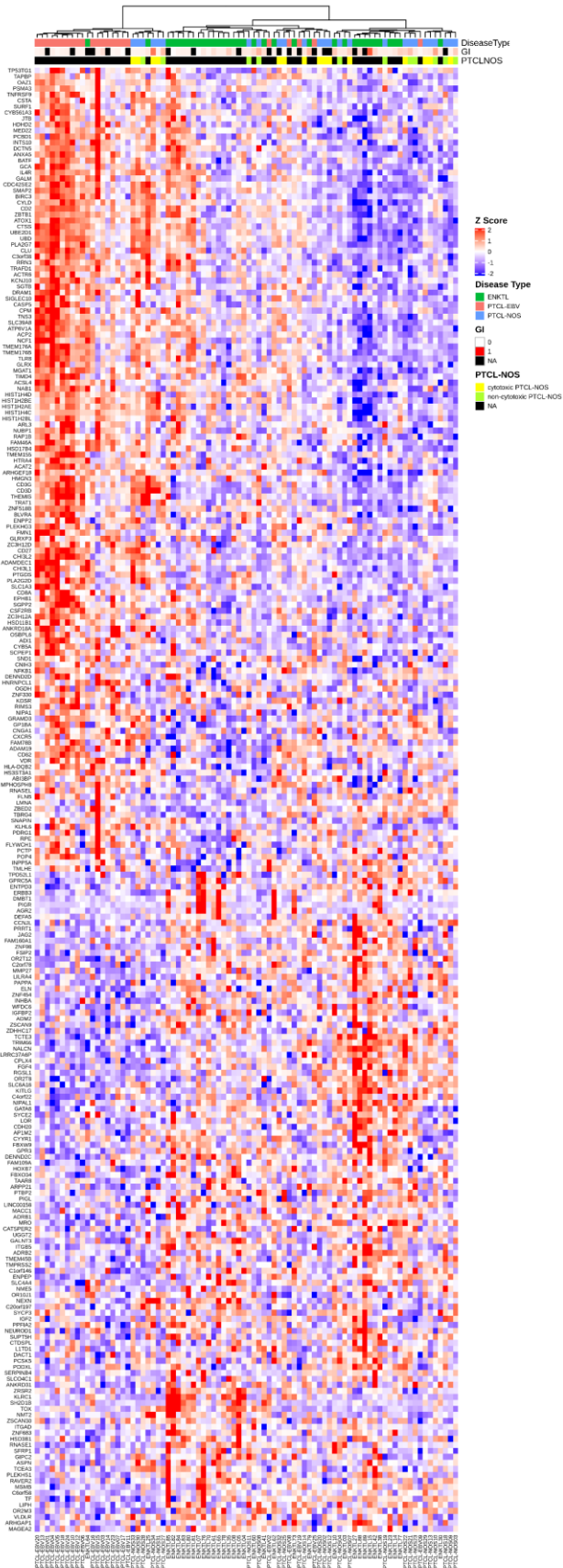
Supplementary Figure 4. Hierarchical clustering heatmap for differentially expressed genes among three disease groups. Expression values for each CCDS gene (row) are normalized across all samples (columns) by Z-score. Upregulation and downregulation of gene expression are marked by red and blue, respectively. Normal P<0.01, adj P (FDR)<0.05 for pairwise comparison among disease groups were used. Three distinct clusters were seen with PTCL-EBV separating from ENKTL and PTCL-NOS. (Refer to Table S8 for complete gene list).

Network Stats	A
number of nodes:	240
number of edges:	209
average node degree:	1.74
avg. local clustering coefficient:	0.347
expected number of edges:	160
PPI enrichment p-value:	0.000121

Network Stats	B
number of nodes:	93
number of edges:	52
average node degree:	1.12
avg. local clustering coefficient:	0.294
expected number of edges:	35
PPI enrichment p-value:	0.00402

Supplementary Figure 5. STRING analysis of proteomics data among three disease groups. Network statistics reporting data concerning the number of nodes and edges, the average node degree, the average local clustering coefficient, the expected number of edges and the protein-protein interaction (PPI) enrichment p-value in comparison between (A) PTCL-EBV vs ENKTL and (B) PTCL-EBV vs PTCL-NOS.

40
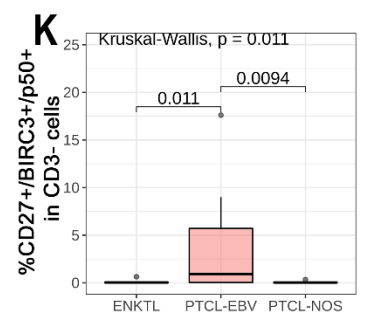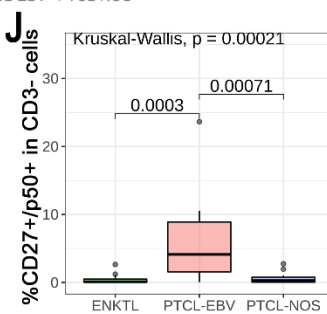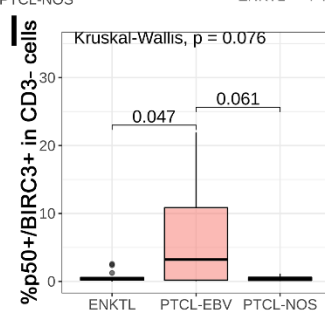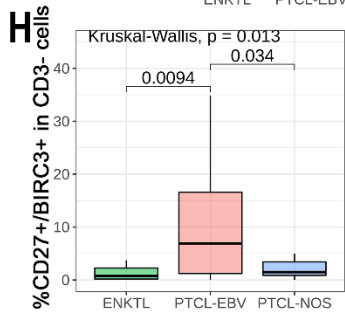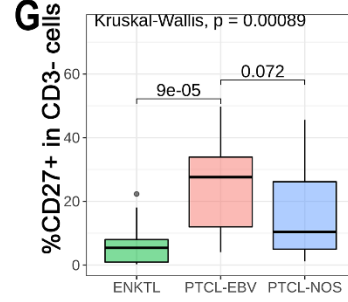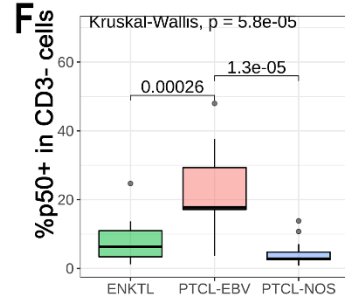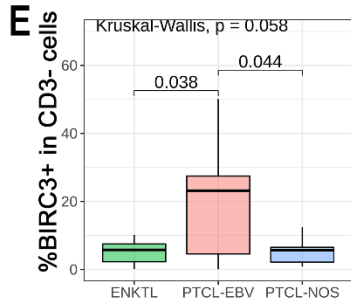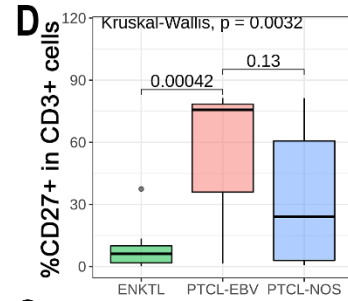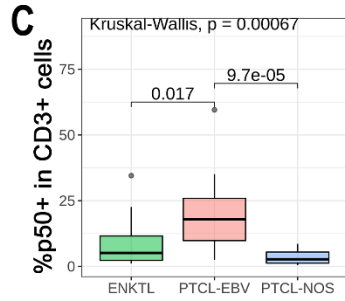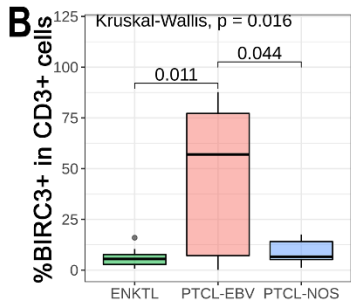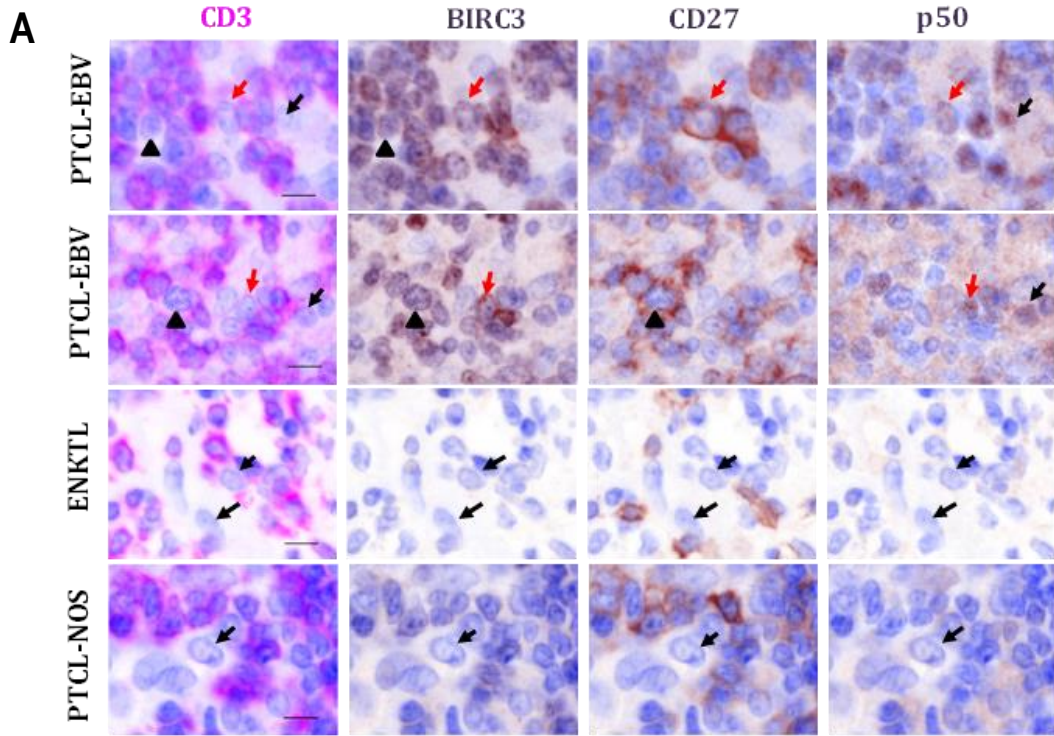
Supplemental Figure 6. Protein expression of CD27, p50, BIRC3 in PTCL-EBV, ENKTL and PTCL-NOS using pseudo-immunohistochemistry images generated from multiplex immunofluorescence images. (A) In PTCL-EBV case, some non-tumour cells (CD3⁻) are triple positive BIRC3⁺/CD27⁺/p50⁺ (red arrow, first row), some are double positive for BIRC3⁺/CD27⁺ (arrowhead, second row) and BIRC3⁺/p50⁺ (red arrow, second row), while a few are single positive for BIRC3 (arrowhead, first row) and p50 (black arrow, first and second rows). In contrast, the non-tumour cells (CD3⁻) in ENKTL and PTCL-NOS are mostly negative for these three markers. (Scale bars represent 20μm.) Boxplots of percentage of BIRC3+, p50+ and CD27+ cells in (B-D) tumor and (E-G) non-tumor cells. Boxplots of percentage of non-tumor cells with double positive (H-J) and triple positive (K) for expression of CD27, p50 and BIRC3. At least four images containing more than 10,000 cells were quantified per case. Our results indicated an increased number of BIRC3+ and p50+ cells in tumor and non-tumor cells of PTCL-EBV compared to other diseases. The percentage of CD27+ cells is significantly higher in tumor and non-tumor cells of PTCL-EBV compared with ENKTL but not with PTCL-NOS. Non-tumor cells with CD27/BIRC3 and CD27/p50 double positive as well as CD27/p50/BIRC3 triple positive are also significantly higher in PTCL-EBV compared to ENKTL and PTCL-NOS.
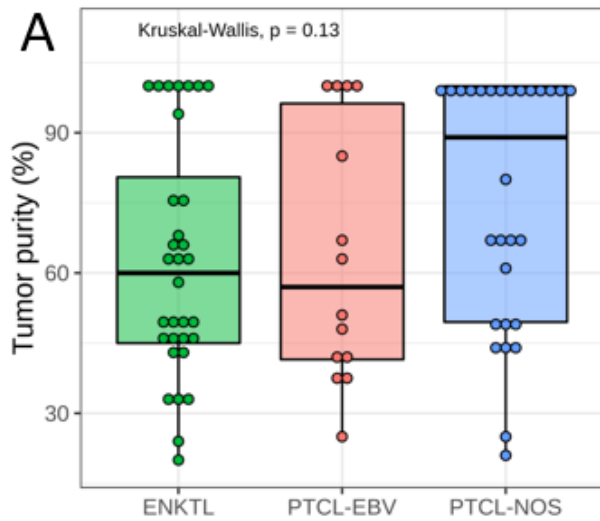
Supplemental Figure 7. Comparison of tumor content and tumor microenvironment (TME) compositions between the three disease groups. (A) There is no significant difference in tumor content amongst the 3 disease groups. (B) For TME, the proportion of immune cell types was determined by deconvolution of normalized transcriptome using CIBERSORTx. The cosine similarity values for the three group pairs, ENKTL vs PTCL-EBV, ENKTL vs PTCL-NOS and PTCL-EBV vs PTCL-NOS are 0.992, 0.983 and 0.979, respectively. These cosine similarity values indicate the three disease groups are globally highly similar or rather homogeneous in the compositions of the main immune cell components.
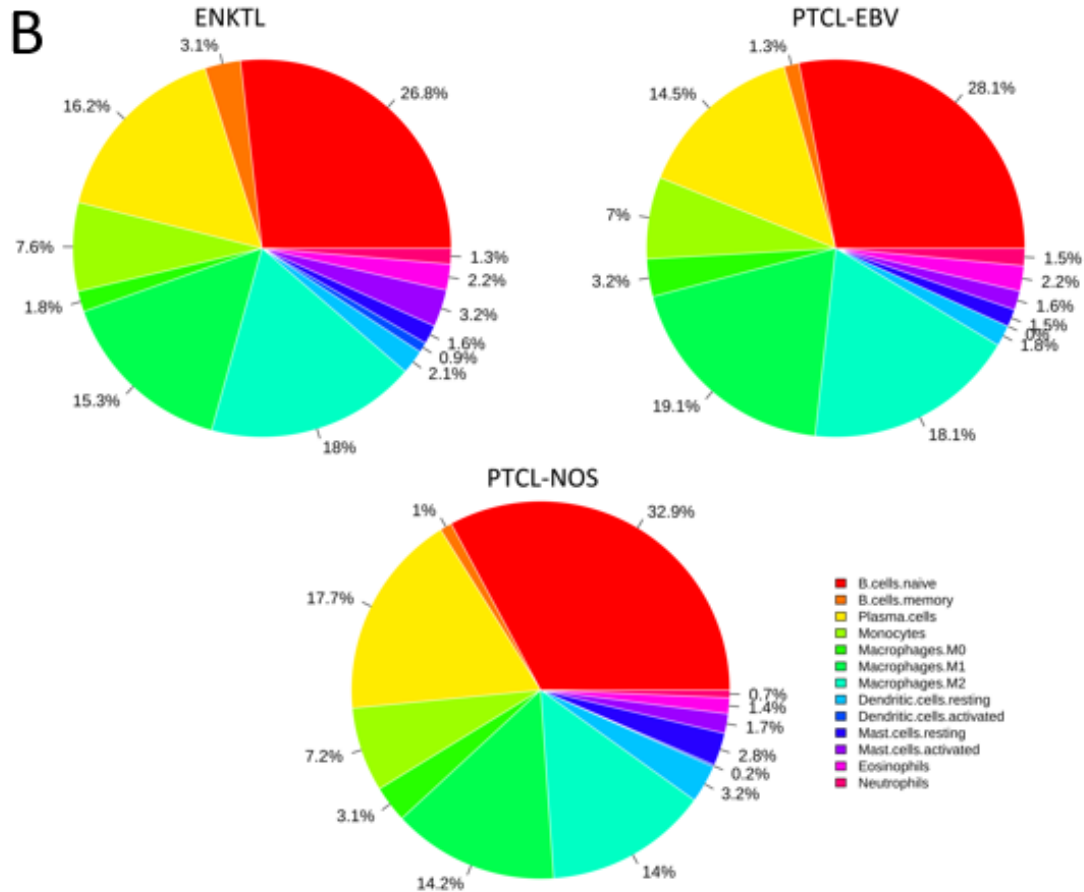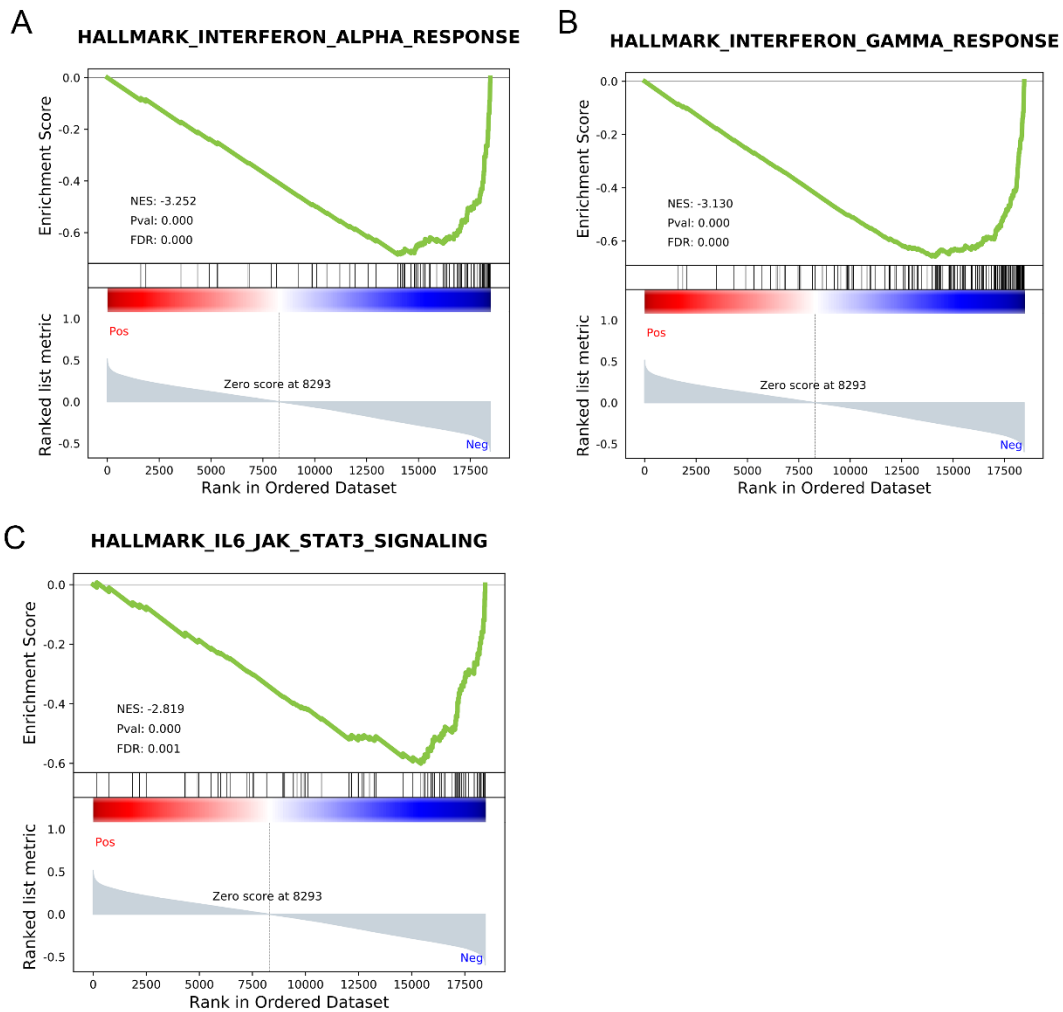
Supplementary Figure 8. GSEA enrichment plots of top three gene sets from GSEA analysis (see Supplementary Table 11). (A) IFN-α response, (B) IFN-γ response and (C) IL-6/JAK/STAT3 pathway.
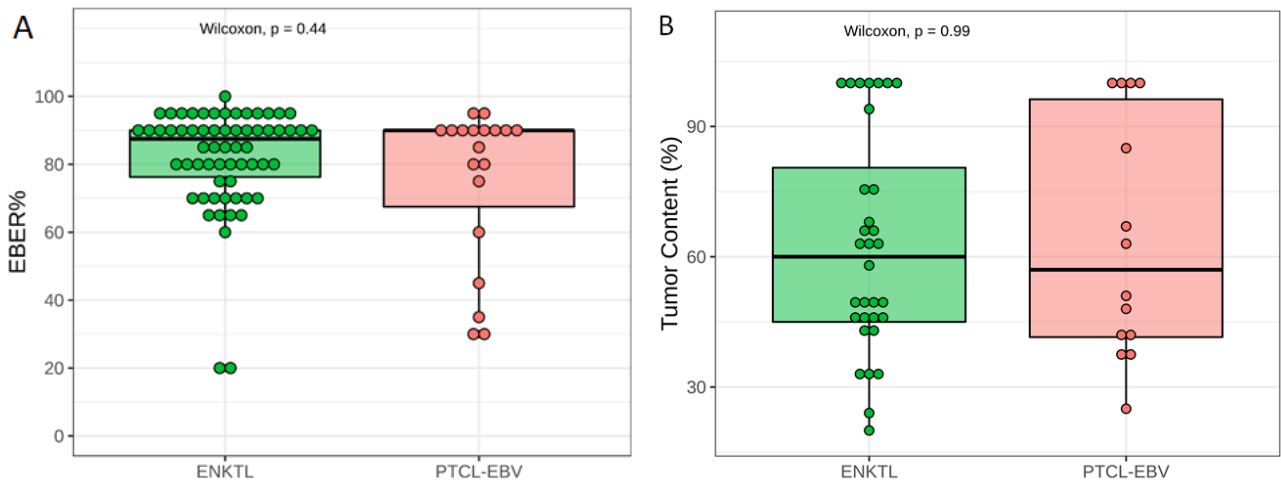
Supplementary Figure 9. Comparison of EBER positivity and tumor content between ENKTL and PTCL-EBV. No significant difference in the EBER expression (A) and tumor content (%)(B) was observed between ENKTL and PTCL-EBV.
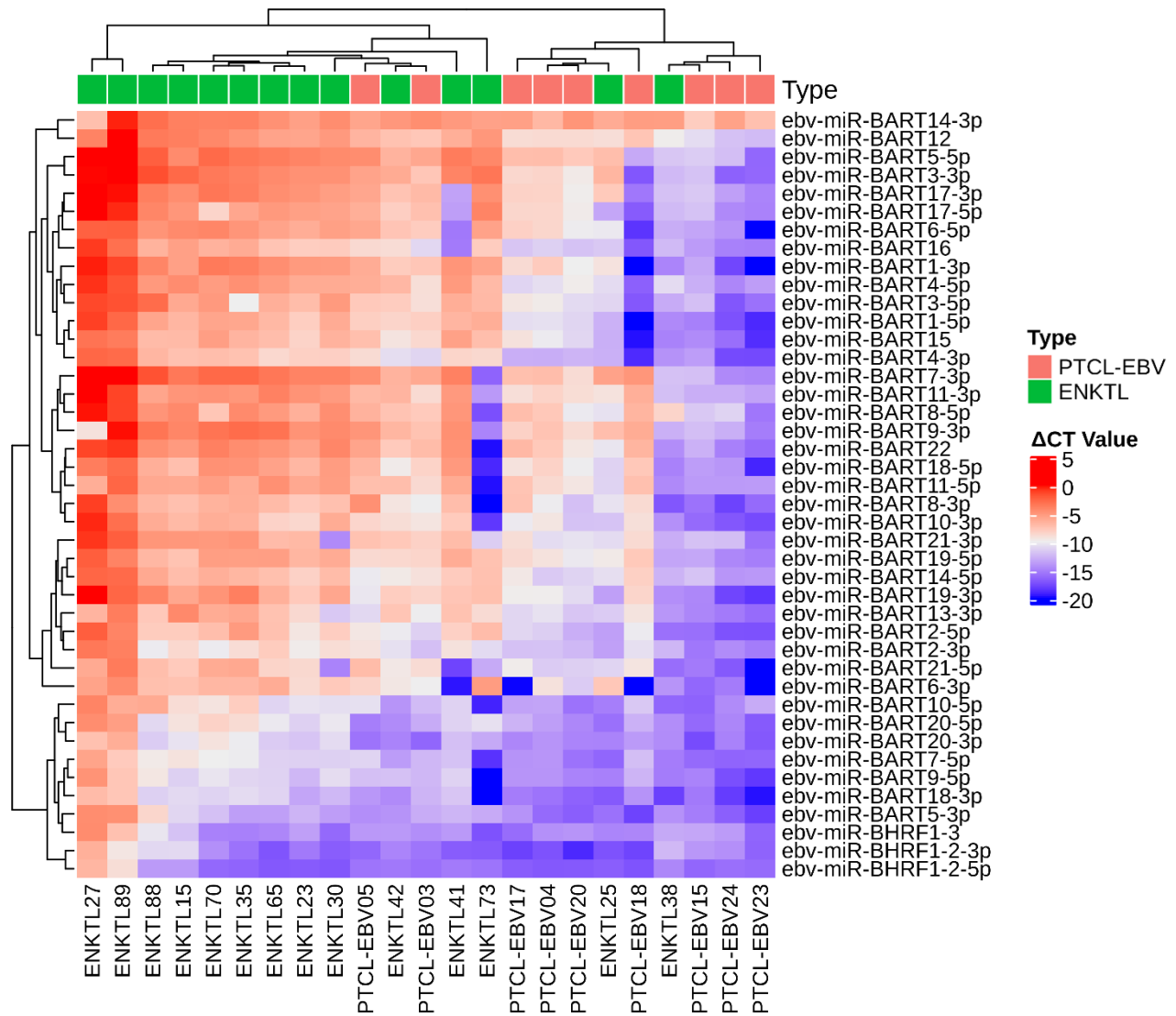
Supplementary Figure 10. Expression of EBV miRNAs in PTCL-EBV and ENKTL. PTCL-EBV exhibited a distinct cluster from ENKTL and showed lower expression in 76% (32/42) EBV miRNAs compared to ENKTL (Table S13). Each column represents a case. Ct values were normalized to housekeeping genes and represented as ΔCt (Ct[reference]-Ct[gene of interest]). Red denotes high and blue denotes low expression levels.
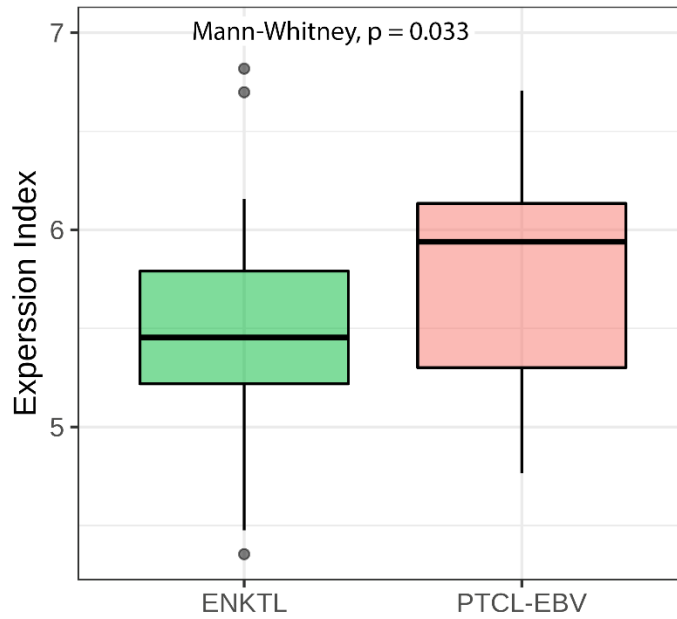
Supplementary Figure 11. Gene set Expression Index of ENKTL and PTCL-EBV. Gene set expression index indicates median expression value of the negatively correlated mRNA target genes of differentially expressed EBV-miRNA between ENKTL and PTCL-EBV. We observed a higher expression index in PTCL-EBV compared to ENKTL.
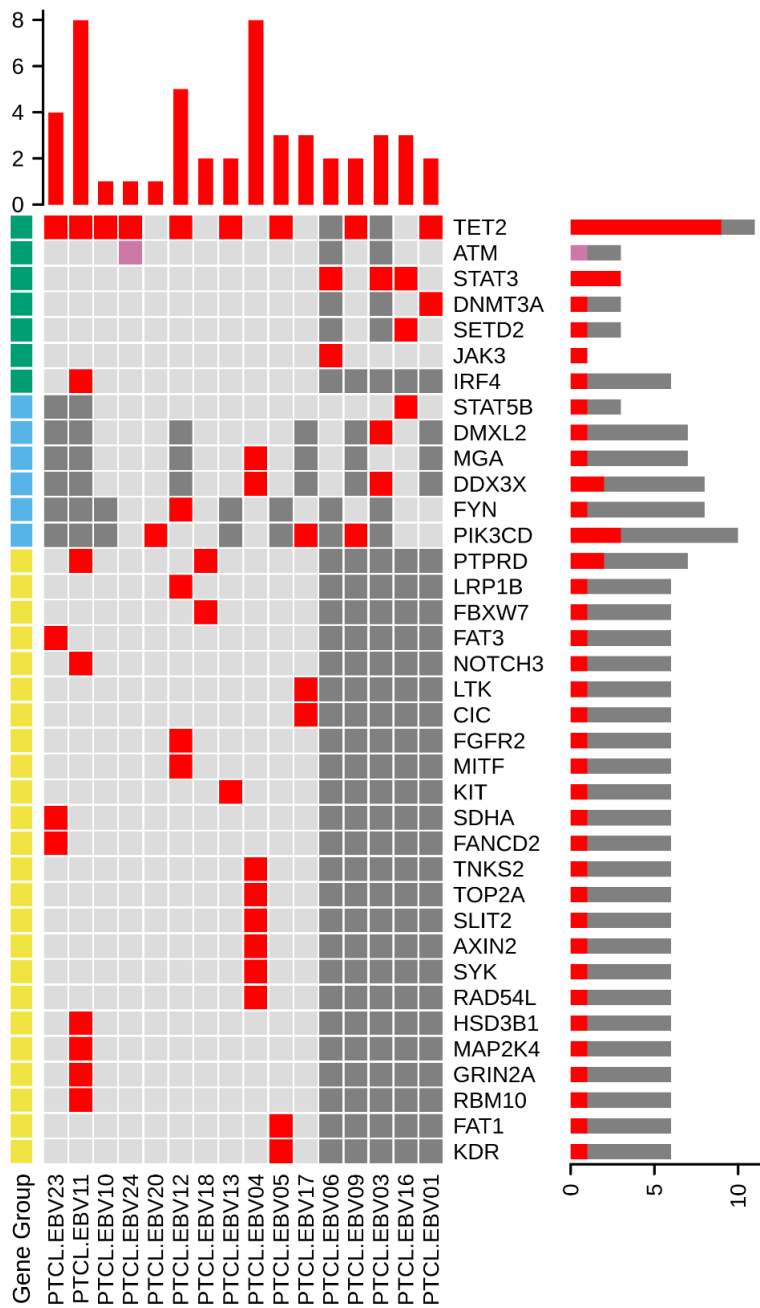
Supplementary Figure 12. Mutational analysis of PTCL-EBV. Mutational analysis of PTCL-EBV using a 35-gene T/NK lymphoid panel and a 484-gene NovoPM™ 2.0 assay (total 500 genes with 19 common genes covered in both panels). The most commonly mutated gene is TET2 (9/14, 64%) followed by PIK3CD (3/9, 33%), STAT3 (3/16, 19%), DDX3X (2/10, 20%) and PTPRD (2/11, 18%). Only genes with at least one mutation detected are represented in the map. Genes without mutation detected in either panels are excluded. Refer Table S3A,B for the complete lists of genes tested.
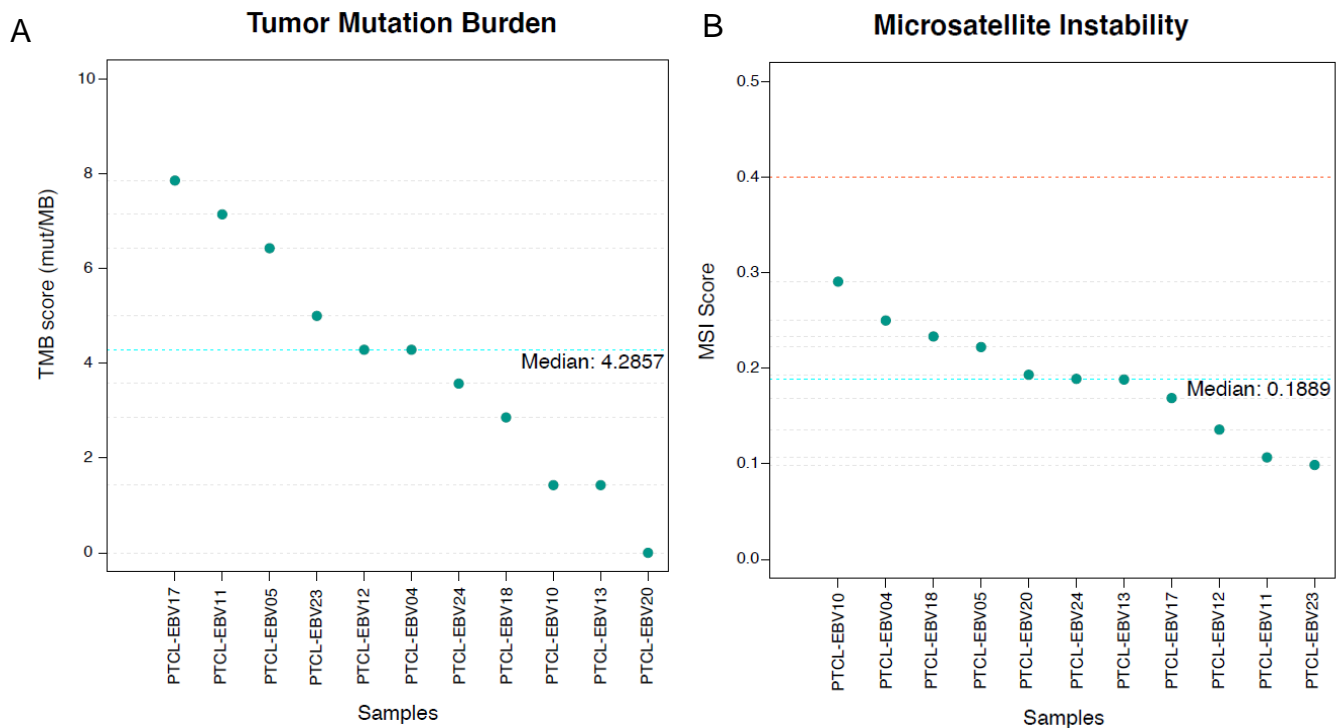
Supplemental Figure 13. Genome stability analyses in PTCL-EBV by NovoPM™. (A) Tumor Mutation Burden (TMB) analysis showed PTCL-EBV samples have a median mutation score of 4.286 mut/MB (range 0 to 7.86 mut/MB). (B) Microsatellite instability (MSI) analysis showed that all 11 samples had microsatellite instability score (MSI) score below the threshold score of 0.4 (median 0.189) and are regarded as microsatellite stable (MSS).
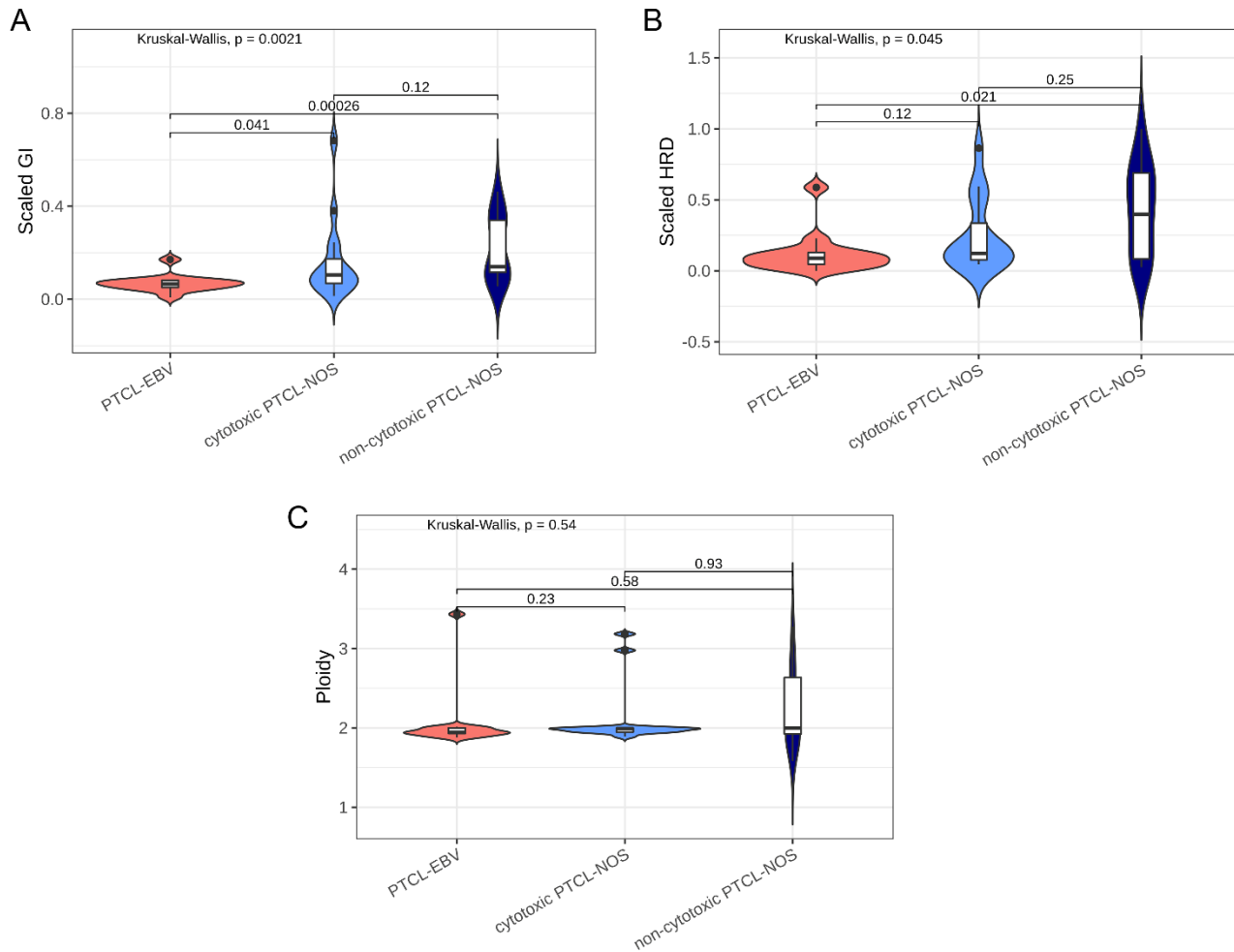
Supplemental Figure 14. Comparison between GI-, HRD- and ploidy scores across PTCL-EBV, cytotoxic PTCL-NOS and non-cytotoxic PTCL-NOS. There is no difference in (A) GI-, (B) HRD- and (C) ploidy scores between cytotoxic and non-cytotoxic PTCL-NOS. There is a significant difference in GI- but not HRD-score between PTCL-EBV and cytotoxic PTCL-NOS. PTCL-EBV showed significantly lower GI- and HRD- scores compared to non-cytotoxic PTCL-NOS. There is no significant difference in ploidy score among the three groups.
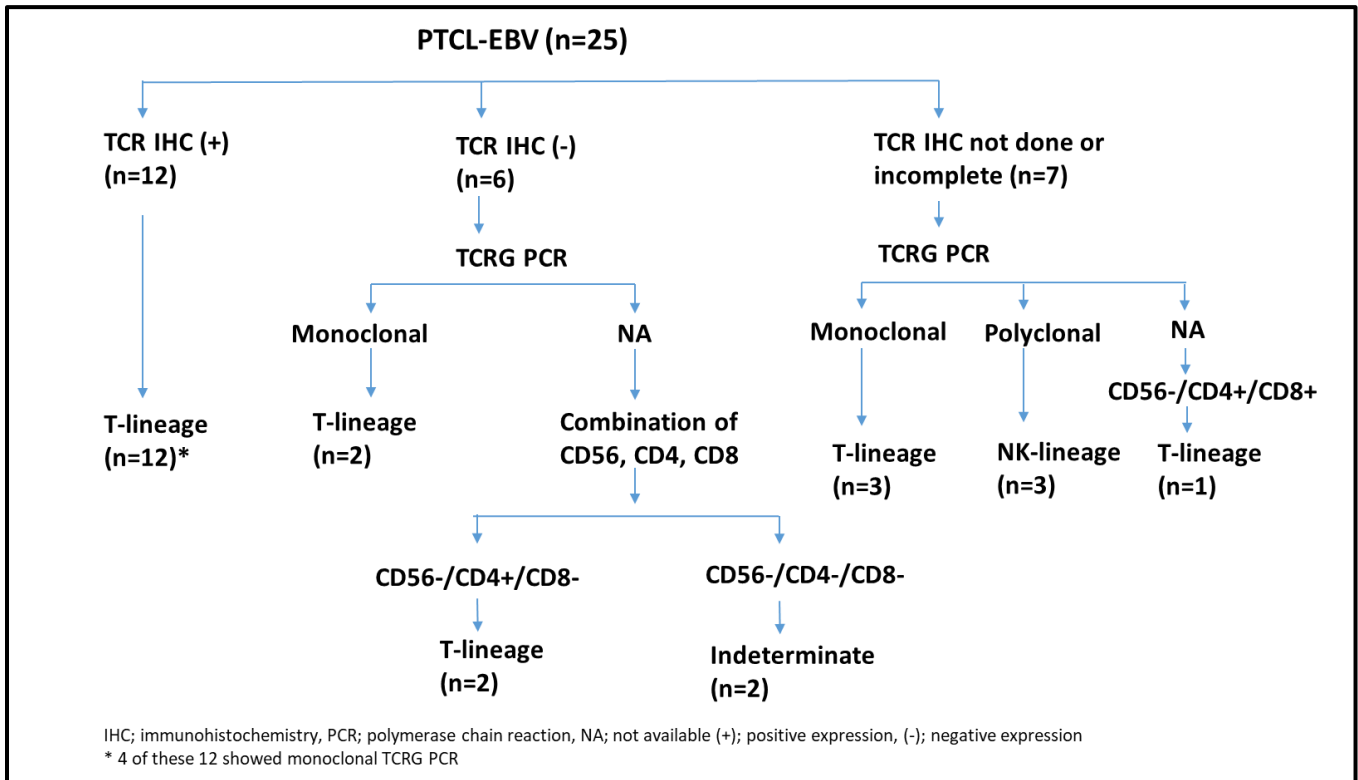
Supplemental Figure 15. Flow chart illustrating the determination of T vs NK-cell lineage. T vs NK-cell lineage was determined based on the expression of TCRβ and TCRγ immunohistochemistry and clonality for TCRγ gene rearrangement by PCR. Cases with negative expression for TCRB/TCRG IHC and lacking clonality data had lineage assignment based on combination of CD56, CD8 and CD4 expressions.